Fall 11-29-2018

Nanostructured cobalt sulfide for energy generation and storage applications: Effect of cobalt sulfide phase on electrochemical properties

May Yousef Altammar
Pittspurg State University, maltammar@gus.pittstate.edu

NANOSTRUCTURED COBALT SULFIDE FOR ENERGY GENERATION AND ENERGY STORAGE APPLICATIONS: EFFECT OF COBALT SULFIDE PHASE ON ELECTROCHEMICAL PROPERTIES

A Thesis Submitted to the Graduate School
in Partial Fulfillment of the Requirements
for the Degree of
Master of Science

May Altammar

Pittsburg State University

Pittsburg, Kansas

December, 2018

NANOSTRUCTURED COBALT SULFIDE FOR ENERGY GENERATION AND ENERGY STORAGE APPLICATIONS:
EFFECT OF COBALT SULFIDE PHASE ON ELECTROCHEMICAL PROPERTIES

May Altammar

APPROVED:

Thesis Advisor: _____
Dr. Ram Gupta, Department of Chemistry

Committee Member: _____
Dr. Khamis Siam, Department of Chemistry

Committee Member: _____
Dr. Pawan Kahol, Department of Physics

Committee Member: _____
Dr. John Franklin, Department of English and Modern Languages

ACKNOWLEDGEMENTS

Every minute in my scientific journal, every second in the study of master degree, I did not stop thanking Allah almighty until the moment of writing this thesis paper. In the first place, thanks to Allah for the inspiration, erudition and positive energy to complete this project duly.

I owe my profound gratitude to those who assisted me to pass all the difficulties that I faced through preparing the master degree. The secret of my successful study with unlimited silent support, who handle the study path to the end with me, is my dear husband Osama. This achievement would not have been imaginable without him. Also, I would like to thank the sources of inspiration, who helped me to light up all nights to climb the ladder of science: my parents. Thank you for advising me with encouragement toward the completion of my master's degree.

I would like to extend my appreciation to my thesis advisor Dr. Ram Gupta. I heartily thank him; the door of Professor Gupta's office was always open whenever I had a misunderstanding about my project or concerns about my thesis writing. His guidance, support, colossal knowledge and stimulus were always available for me.

Moreover, I would like to express sincere regards to all my committee members: Professor Khamis Siam, Professor Pawan Kahol and Professor John Franklin of the English department and all other faculty members in the Chemistry Department at Pittsburg State University. Additionally, I would like to thank the University of Kansas at Lawrence for recording SEM image and XPS analysis.

Finally, I cannot forget to thank my children Rayyan and Latifah. It is my respect and good fortunate to extend this success to them: their smiles, accomplishments, energy

and their youthfulness supported me and contributed to making the adversities that I faced throughout these two years' journey much easier. I hope this work is a moment of pride for them in fut

NANOSTRUCTURED COBALT SULFIDE FOR ENERGY GENERATION AND ENERGY STORAGE APPLICATIONS:
EFFECT OF COBALT SULFIDE PHASE ON ELECTROCHEMICAL PROPERTIES

An Abstract of the Thesis by
May Altammar

Increasing global population has caused increased energy demand for our daily needs such as household appliances, portable electronic devices, automobiles, aerospace vehicles and industrial equipment. It is an urgent need of our current technological world to produce and store the energy efficiently and in an eco-friendly way. Fuel cells and supercapacitors are among widely used energy conversion and storage devices. To meet our growing needs, this thesis is extensively focused towards advanced energy material with multifunctional capabilities to act as remedial solutions for energy generation and storage material. In this work, nanostructured cobalt based oxides, hydroxides and sulfides were synthesized using a facial hydrothermal method. Phase purity and physical morphology of the synthesized materials were characterized using X-ray diffraction spectroscopy (XRD) and scanning electron microscopy (SEM), respectively. The electro catalytic performance of the cobalt based materials were analyzed for supercapacitor and water splitting application. The properties of supercapacitance were measured by using a three-electrode system. Galvanostatic charge-discharge (CD) and cyclic voltammetry (CV) process were used to investigate the energy storage capacity, while electrocatalytic water splitting activities were studied by cyclic voltammetry, linear scanning voltammetry (LSV) and electrochemical impedance spectroscopy (EIS).

The optimized cobalt based materials cobalt sulfide Co_3S_4 exhibited outstanding electrochemical stability with maximum specific capacitance of 12.751 mF/cm^2 at 2 mV/S.

The best sample of cobalt based materials showed excellent stability for 5,000 cycles of the charge-discharge study with almost 100% charge retention and coulombic efficiency. In contrast, the electrochemical properties toward hydrogen and oxygen evaluation reactions required low over-potential of 217 mV and 126 mV at 10 mA/cm^2, respectively. Hence, from this work we observed that cobalt sulfide Co_3S_4 could be a promising multi-functional material for high performance, durable energy generation and storage devices.

Table of Contents

CHAPTER
PAGE

List of Tables

List of Figures

CHAPTER I

INTRODUCTION

1.1 Renewable energy:

The growing population around the world and consumption of fuel energy have caused a rapid increased of global warming, air pollution, and environmental issues. The power demand has been running ahead of supply and the electricity requirements are swelling at an alarming rate.[1] With highly dependence of life on technology, energy storage and generation is in need. Nowadays, scientists are becoming more interested in searching for alternative energy sources particularly renewable energy for example, energy independence and energy security. The German Federal Government [2] has set itself the objective of generating total electricity the country needs from sun, wind, biomass, by 2050.[2] In spite of the eminent potential of renewable energy resources like solar power, wind and geothermal, their applications could be limited due to the reliability of supply which means the renewable energy reckons on the weather conditions for its source of power.[3,4] Therefore, powerful, sustainable energy storage devices are necessary to their applications. Hence, i good options to overcome the negative impact of conventional resource are required.

1.2 Need for energy storage application:

With the expansion in energy claimed, enhancing low-cost, eco-friendly,

sustainable, and efficient energy storage and generation technologies have become one of the desired approaches for the energy science and technology. Amongst various energy storage, electrochemical ones such as fuel cells, batteries and supercapacitors have been recognized as significant energy storage applications. Particularly, supercapacitors have to be considered because of their characteristics and functional electronic features.

1.2.1 Supercapacitor:

A supercapacitor also known as an ultracapacitor is one of the challenges energy storage device.[5] The mechanism of operation is similar to a conventional capacitor. It consists of two electrodes but the difference is that the two electrodes are separated by an electrolyte instead of solid dielectric.[6] Supercapacitors integrate the properties of energy storage of batteries with the characteristics of power discharge of capacitors. Consequently, supercapacitors can produce greater energy densities than conventional capacitors and higher power densities than fuel cells and batteries.[7] Therefore, supercapacitor technology gives an access to fill the gap between capacitor and battery as shown in Figure 1.1.

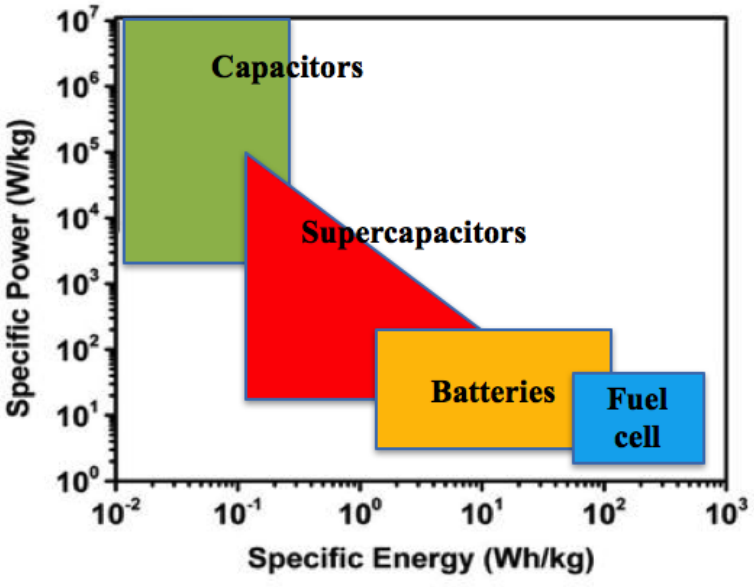

Figure 1.1: Ragone plot for energy density versus power density.

In the matter of classification of supercapacitance based on charge-storage mechanism, there are two types of supercapacitors: electrochemical double layer capacitors EDLCs and pseudo capacitors. In EDLCs, the mechanism of storage charge utilizes electrode/electrolyte interfaces. Hence, the difference in the potential across EDLCs stimulates different polarity of the electrode, which induces electrolyte ions to migrate to the electrode microporous. So, the capacity in EDLCs relays an electrostatic charge controlled by the thickness of the double layer at the electrode/electrolyte interface (non-faradic reaction).[7] Activated carbon material is used in this kind of supercapacitance. Nevertheless, the capacitor in pseudocapacitors depends on electrochemical faradic reactions.[7] Fast reversible oxidation /reduction faradic reaction can provide 10-100 times more than pure- carbon based EDLCs.[7,8] Because of their pseudocapacitive property to give excellent capacity, conductive polymers and nonprecious transitional metal such as cobalt oxide, nickel oxide are usually used as electrode material. When electrochemical double layer capacitors and pseudocapacitors are used, they lead to hybrid capacitors.

In general, the key attributes making supercapacitors more engaging as promising energy storage devise are long cycle life, fast charge-discharge, and wide operating temperature scope, higher power density than battery and larger energy density than conventional capacitors. In spite of all these advantages, supercapacitance is still suffering from low energy density. This challenge has spotlighted supercapacitance for future energy storage applications.

1.2.2 Water splitting and energy:

Nowadays, modern society and advanced technology are involved in an unorthodox accretion rate of imitative fuel cell use. Environmental hazard and emitting of those carbon

fuels have motivated the scientific community to discover green energy.

Water splitting is effective method to generate energy and meet the features of zero carbon emission, because it is eco-friendly, and has everlasting fuel cell energy. Water splitting results in two half-cell reactions, hydrogen evaluation reaction at cathode and oxygen evaluation reaction at anode respectively as following:[9]

$2H\,(aq) + 2e^{-} \rightarrow H_2\,(g)$……(1)

$2H_2O\,(l) \rightarrow O_2\,(g) + 4H^{+}\,(aq) + 4e^{-}$ ……. (2)

However, thermodynamically, because water splitting takes place at overpotential of 1.23 V (vs. RHE) for OER and zero V (vs. RHE) for HER, both oxygen and hydrogen evaluation reactions are restricted by the low electrocatalytic efficiency and high overpotential. Furthermore, the feasible implication of this technology is limited by the rarity of active earth metal-based catalysts.[10,11]

Recently, water electrolysis is a sector where the technology required to be developed overcomes the high overpotential. Transition metal oxides, hydroxides, phosphides, and sulfides such as CoS, MoS_2, NiO and CoOH are being utilized as sustainable, cost affective and alternative catalysts for noble metals.[9] Figure 1.2 demonstrates the schematic of water electrolysis to generate green energy.

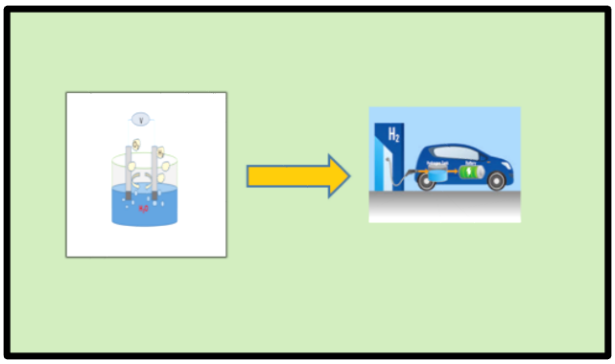

Figure1.2: Schematic of water electrolysis to generate energy.

1.3 An efficient material for energy storage and generation applications:

1.3.1 Cobalt oxide:

In recent years, cobalt oxides have captivated an enormous amount of attentiveness for extended technology applications involving sensing and electronic, biomedical devices and electrocatalysts for the oxygen evolution reaction.[12] Also, cobalt oxides have attracted great attention in capacitive behavior. Using cobalt oxides as functional electrode in supercapacitors are becoming increasingly an efficient route.[13] These features of cobalt oxides could be assigned to multiple redox phases CoO, Co_2O_3, and Co_3O_4, with their properties, such as excellent electrochemical performance, high saturation magnetization and stable catalytic activity.[12] Moreover, recent research has focused on Co_3O_4 to enhance the electrochemical property for energy storage and generation applications since the Co_3O_4 possesses a theoretical specific capacitance of (3560 F/g).[13,14,15,16,17]

1.3.2 Cobalt sulfide:

With demand growing for high efficient electronic devices for supercapacitors and energy generation, cobalt sulfide has been considered as a dynamic material as an electrode toward great mechanism for supercapacitance and energy generation.[18,19] Noteworthy electrochemical properties of cobalt sulfide could be utilized in various potential applications such as charge storage devices, catalysts, solar cell as counter electrode, and advance Li-ion batteries.[18,20,21]

Over the last view years, the scientific community has focused on cobalt sulfides since cobalt sulfides own different faces of Co_4S_3, Co_9S_8, CoS_2, Co_3S_4, $Co_{1-x}S$, Co_2S_3,

which can play an extensive role in fast-improving domain of new energy devices. Multiple and fast charge/discharge cycles make cobalt sulfides promising material for energy generation and energy storage applications. [22,23,24]

Moreover, Hu et al. recorded that nanostructure and morphology of cobalt sulfides could have an effect on the electrochemical performance of the phase.[25] Cobalt disulfide CoS_2 nanoparticles and cobalt sulfide CoS nanoflakes were synthesized by using facial solvothermal method. Sulfur powders and thiourea were consumed in synthesize. In addition, it was realized that there is no impact of the amount of thiourea on their phase structure, but the influence only was on their morphology's impact. Regular hexagonal shape and single-crystalline cubic structure were observed corresponding to CoS nanoflakes and CoS nanoflakes respectively.

As more evidence, Esam Alqurashi,[26] synthesized hollow structured cobalt sulfide in a hydrothermal process. The result showed the obtained electrode hexagonal $Co_{1-x}S$ phase of cobalt sulfide exhibited a Tafel slope of 97 mV per decade as an electrocatalyst for hydrogen evaluation reaction. Specific capacitance from cyclic voltammetry test was 867 F/ g at 5 mV/ s. The specific capacitance was retained even after 5000 charge–discharge cycles. All these results confirm unique and stable electrochemical performance of $Co_{1-x}S$ for future energy application.

In addition, crystallinity, morphology, pore structure and nanoparticles have obtained remarkable attention to develop electrochemical property of the electrode. Xueting,[27] has successfully fabricated cobalt pentlandite Co_9S_8 in a one-step solvothermal process. The SEM result indicated to hollow sphere nanostructure phase of Co_9S_8. This nanostructure could be explained by a large surface area and stellar electrocatalytic performance for

oxygen evaluation reaction. A nitrogen adsorption−desorption test was used to illustrate the pore distribution of the structure. The hollow spheres displayed intense pore distribution with a size of 4.3 nm. The hollow spheres showed a significant overpotential of 285 mV at 10 mA cm^{-2} with Tafel slope of 58.0 mV/decade, which means the morphology of Co_9S_8 could accord profuse electroactive positions for reversible adsorption of oxygen on the catalyst surface and noteworthy short pathway diffusion of the electrolyte. So, outstanding electrochemical performance of different phases of cobalt sulfides is highly dependent on their morphology, size, porosity and pore size distribution

1.4 Theme of this research:

The theme of this research is to use facial hydrothermal process to synthesize multifunctional nanostructured cobalt- based materials for energy generation and storage applications. Furthermore, another objective of this research is to investigate the effect of cobalt sulfide phase on electrochemical properties. Cyclic voltammetry, Galvanstatic charge-discharge measurements, electrochemical impedance spectroscopy, and linear sweep voltammetry were studied in accurate details toward electrochemical properties for supercapacitor and water catalysts.

CHAPTER II

EXPERIMENTAL DETAILS

2.1 Materials:

The substances required to synthesize different faces of cobalt- based material were Cobalt acetate tetra hydrate $Co(Ac)_2 .4H_2O$ (Acros organics), Ethylene glycol $C_2H_6O_2$, thiourea $(NH_2)_2CS$ (MP Biomedicals, LLC), and urea$(NH_2)_2CO$ (Fisher Sci) and deionized (DI) water. In addition, for electrode fabrication Ni-foam, acetylene black, polyvinylidenedifluoride (PVdF), N-methyl pyrrolidinone (NMP) were used. All chemical materials were utilized without further purification.

2.2 Synthesize different face of nanostructure cobalt sulfide:

Several faces of cobalt sulfide CoS were prepared by using the facile hydrothermal method. First three samples **(**5 mM = 1.245 g) of cobalt acetatetetrahydrate [$Co(Ac)_2$ **)** $.4H_2O$] were dissolved in three beakers of 30 ml ethylene glycol and then different weight of thiourea (5 mM = 0.381 g), (10 mM = 0.762 g), (15 mM = 1.143 g) were dissolved in the same solutions respectively . The entire solutions were transferred to three of a 45 ml Teflon lined autoclave having a pre-cleaned Ni foam. Then the autoclaves were maintained at 190 °C for 8 hrs and then cooled down to room temperature naturally. The Ni foams were taken out and the powder was filtered using vacuum filtration and washed several times with DI water. The powder was dried at 60 °C for 6 hrs.

2.3 Synthesis of nanostructured cobalt oxide:

Cobalt oxide was synthesized by using the facile hydrothermal method. Cobalt acetate tetra hydrate [$Co(Ac)_2.4H_2O$] was first dissolved in 30 ml ethylene glycol and then urea was dissolved in the same solution. The entire solution was transferred to a 45 ml Teflon lined autoclave having a pre-cleaned Ni foam. The autoclave was maintained at 190 °C for 8 hrs and then cooled to room temperature naturally. The Ni foam was taken out and the powder was filtered using vacuum filtration and washed several times with DI water. The powder was dried at 60 °C for 6 hrs. Half of the powder and one nickel foam was calcined at 350 °C (5 °C/min) for 6 hrs. The details of materials synthesis are explained in Table 2.1.

Table 2.1: Experimental details of cobalt based materials synthesis

Sample code	Cobalt acetate tetra hydrate (g)	Ethylene glycol (ml)	Urea (g)	Thiourea (g)
Co_9S_8 (S1)	1.245	30	_	0.381
Co_3S_4(S2)	1.245	30	_	0.762
Co_3O_4	1.245	30	0.30	_

2.4 Material characterizations:

X-ray diffraction spectroscopy, X-ray photoelectron spectroscopy and scanning electron microscopy are powerful techniques that have been used to examine the characterizations of the samples synthesized. More specifics details follow:

2.4.1 X-ray diffraction spectroscopy:

The synthesized materials structures ware investigated utilizing a Shimadzu X-ray diffractometer set on the 2θ-θ scan with $CuK_{\alpha 1}$ (λ=1.5406 Å) radiation, which was generating at a current of 30 mA and 40 kV of voltage. In terms of detector and source, 0.2 mm of slits was used. The X-ray radiations were lightening directly on the sample and the diffracted radiations were collected and recorded while the sample was rotated through the angle range of 2θ = 10°−80°. To obtain the geometry, the X-ray detector was designed so that the angle between the detector and the atomic planes was 2θ as shown in Figure 2.1

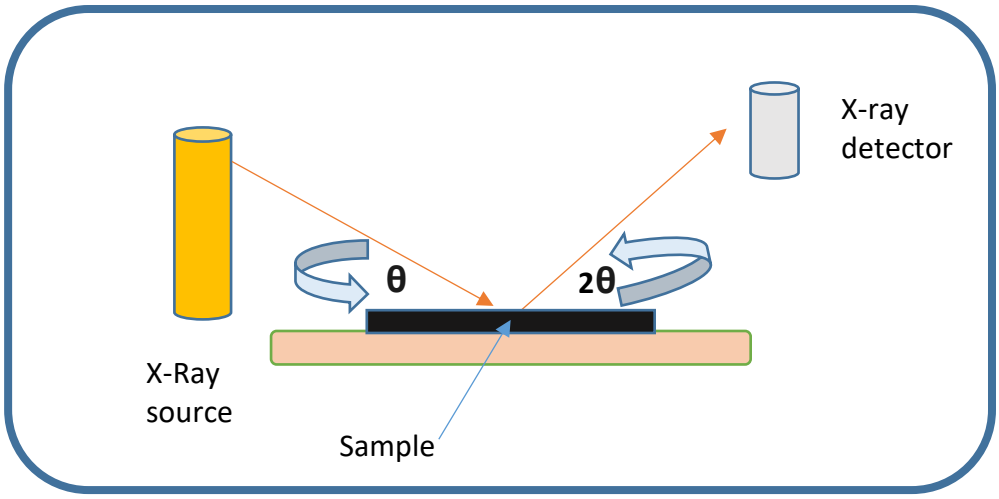

Figure 2.1: Schematic diagram of an X-ray diffractometer.

2.4.2 Scanning electron microscopy:

A topographic technique by scanning electron microscopy was utilized to study the morphology and the physical image surface of the material synthesized. The advantage of using SEM is to demonstrate the formation mechanism for material synthesized in very critical range size micrometers (μm) and nanometers (nm). This assisted the ability to observe and analyze the characterization of each sample clearly.

The shapes and the particle's sizes were provided with the cooperation of the University of Kansas.

2.5 Electrochemical measurements of cobalt-based material for supercapacitor and water splitting:

Electrochemical features of the cell were tested by using a three-electrode system, which contains a working electrode as-synthesized on Ni-foam, a counter electrode as platinum wire and a reference electrode as saturated calomel electrode. The electrochemical properties of the electrode for supercapacitance and water electrolysis have been done in 3M KOH electrolyte and 1M KOH respectively. The schematic diagram of the three electrode system is shown in Figure 2.2.

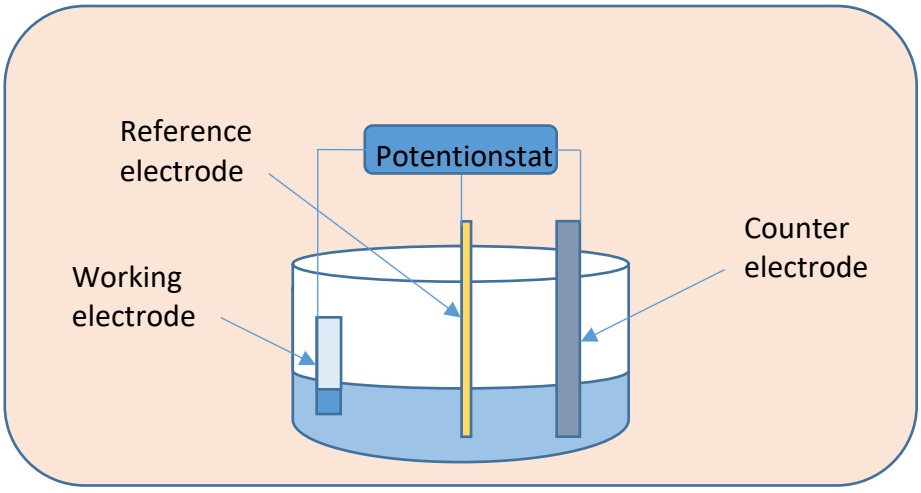

Figure 2.2: Three cell electrochemical measurement system.

Ni-foam was purified using 3M HCl acid then was washed with DI-water before the preparation of the electrode. The cleaned nickel foam was dried in the vacuum oven for 1 h at 60 ^{o}C. Then pure Ni foam was used as in the synthesizing processes for cobalt oxide, S1 and S2 to prepare the working electrode. The area of the electrode was successfully

measured in order to investigate the electrochemical properties of the electrode as supercapacitance and water electrolysis. The electrochemical measurements of all materials synthesis were evaluated at room temperature by utilizing cyclic voltammetry, Galvanostatic charge-discharge, and electrochemical impedance spectroscopy methods, whereas all the electrochemical experiments were driven on a Versastat 4-500 electrochemical workstation (Princeton Applied Research, USA). VersaStudio software provided by Princeton Applied Research was chosen to analyze the electrochemical data. Cyclic Voltammetry technique was used to investigate the charge storage of cobalt-based material as supercapacitor. The experiment was performed at several scan rates of (1-300 mV/s) in a potential range around 0 V to 0.6 V. Galvanostatic charge-discharge measurements were recorded at various current densities of (0.5 - 50) mA/cm^2 in a potential range of (0 - 0.6) V. For EIS, analyses were tested in the frequency range of 0.05 – 10.000 Hz with an amplitude of 10 mV.

In contrast, water electrolysis is considered one of the challenges to generate hydrogen production with low cost and high efficiency electrocatalysts. Thermodynamically, water splitting required 1.23 V in order to drive the reaction as following[28]:

$$2H_2O \rightarrow 2H_2 + O_2 \ldots. (3)$$

Water splitting without an efficient electrode is unfavorable because of the demand to input a large amount of potential energy called overpotential to force the reaction occurs as shown in Figure 2.3. Therefore, oxygen evaluation reaction OER and hydrogen evaluation reaction HER of cobalt-based materials were studied using electrochemical measurements in 1M KOH as an electrolyte. Linear sweep voltammetry, electrochemical

impedance spectroscopy, and chronoamperometry were approached to demonstrate the OER/HER competence of electrode prepared. For OER, The LSV was carried out at a scan rate of 2 mV/s with a potential range of 0.14 – 0.84 V, while the condition of HER was applied at 2 mV/s scan rate in a potential range of (-0.9 – -1.7) V v.s Hg/Hg_2Cl_2.

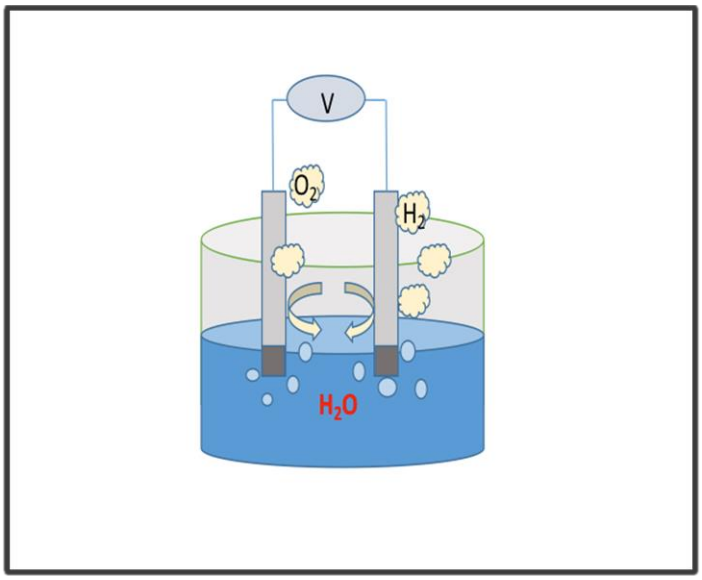

Figure 2.3: Schematic representing water splitting reactions.

CHAPTER III

RESULTS AND DISCUSSION

3.1 Characterization of materials synthesized

3.1.1 X-ray diffraction analysis:

Specific techniques such as powder X-ray diffraction technique were employed to determine the characterization of the hydrothermal synthesized, identification of crystallinity and phase purity. Figure 3.1-3.3 exhibits the XRD pattern of all final material. There are three main diffraction peaks corresponding to (001), (101), and (111) planes indicate uncalcined sample beta-$Co(OH)_2$ structure.[29] All the diffraction peaks in Figure 3.2 show the broad and intense peaks suggesting highly crystalline nature of face-centered cubic structure of Co_3O_4. Moreover, no diffraction peaks appear except Co_3O_4, emphasizing the phase purity of material synthesized after being calcined.[30] Figure 3.3 shows the XRD patterns of the Co_9S_8 and Co_3S_4 synthesized samples. The pattern of Co_9S_8 shows diffraction peaks of (311), (420), (422), (511), (440) and (622) accord with cubic structure of Co_9S_8. Also, no other peaks are detected, indicating the high purity of Co_9S_8.[31] Following the pattern of Co_3S_4, all the peaks are indexed to cubic Co_3S_4 phase. The sharp peak along (311) and (440) planes suggest good crystallinity of the as synthesized materials.[31] As observed from the XRD patterns, Co_9S_8 and Co_3S_4 are crystalline in nature.

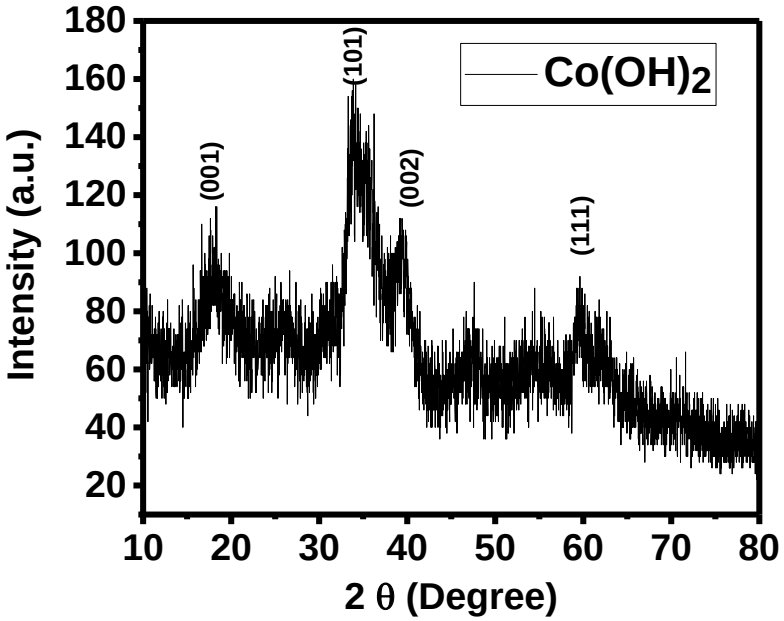

Figure 3.1: XRD patterns of uncalcined $Co(OH)_2$.

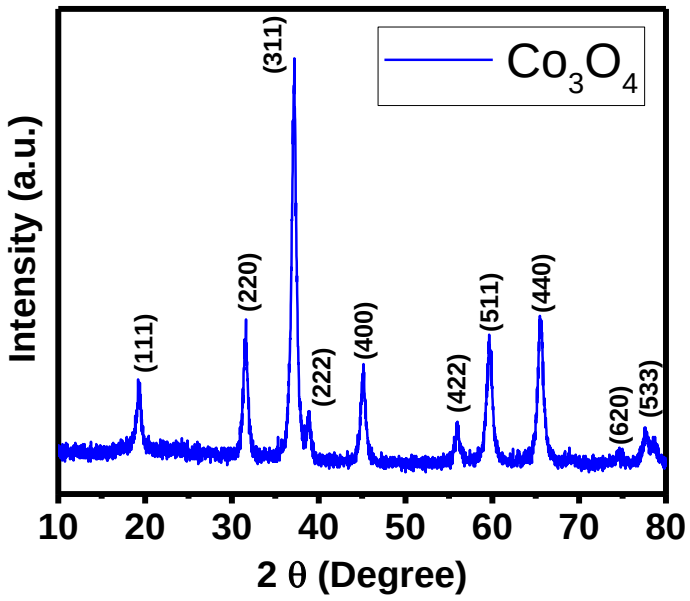

Figure 3.2: XRD patterns of calcined Co_3O_4.

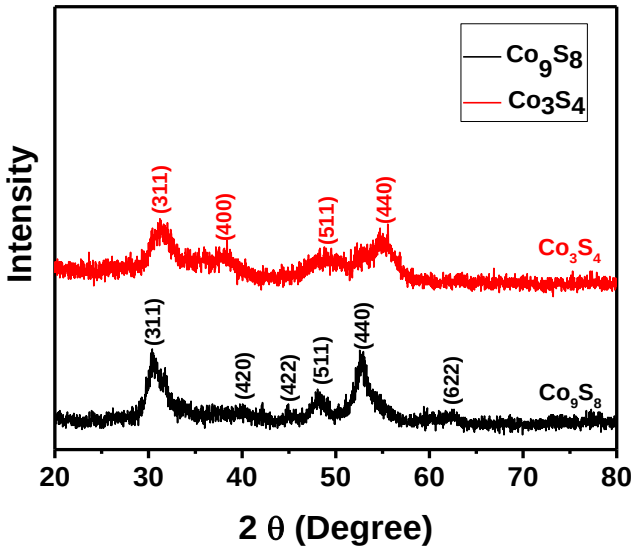

Figure 3.3: XRD patterns of Co_9S_8 and Co_3S_4.

3.1.2 Scanning electron microscopy:

The morphology and structure characterization of cobalt-based materials Co_9S_8 and Co_3S_4 were analyzed in detail using scanning electron microscopy. Figure 3.4 presents SEM image grown on nickel foam. As confirmed in this figure, that cobalt sulfide Co_9S_8 as- synthesized is granular and has nanospherical particles. Figure 3.5 displays mixture of nanospherical and multiple nanocrystal flowers with octahedral edge of Co_3S_4, which can be further confirmed with XRD. Moreover, there is a large area of nanocrystal particles, which can be enable the electrolyte to penetrate the electrode maximally,[32,33] leading to excellent electrochemical properties during the electrochemical measurement. To verify the composition of cobalt sulfide Co_9S_8 and Co_3S_4, energy dispersive X-ray spectrometry was used. Figure 3.6 and Figure 3.7 reveal the homogeneously distributed Co and S over Ni-foam, where carbon, nitrogen and oxygen originate due to the adsorption of the surface from ambient environment.[34]

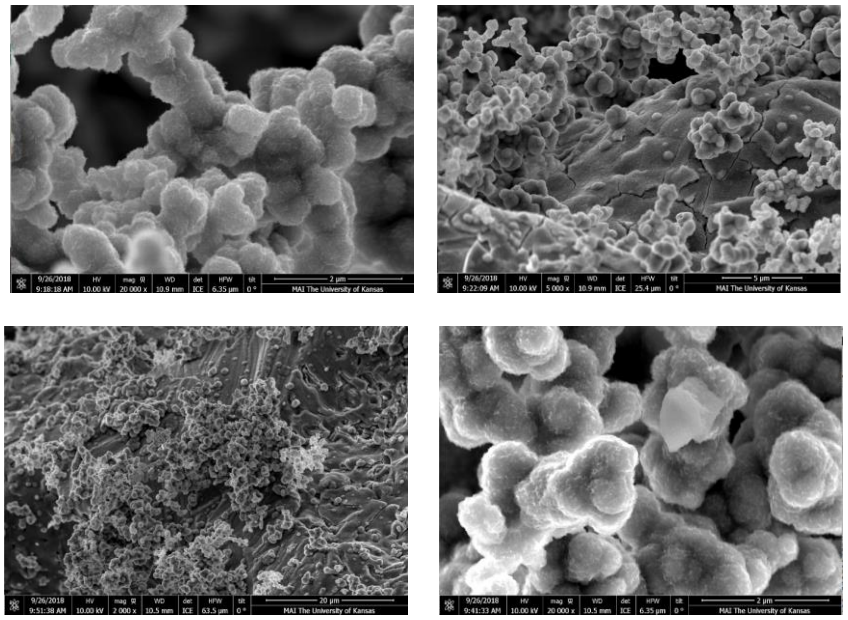

Figure 3.4: SEM images of Co_9S_8 at different magnifications.

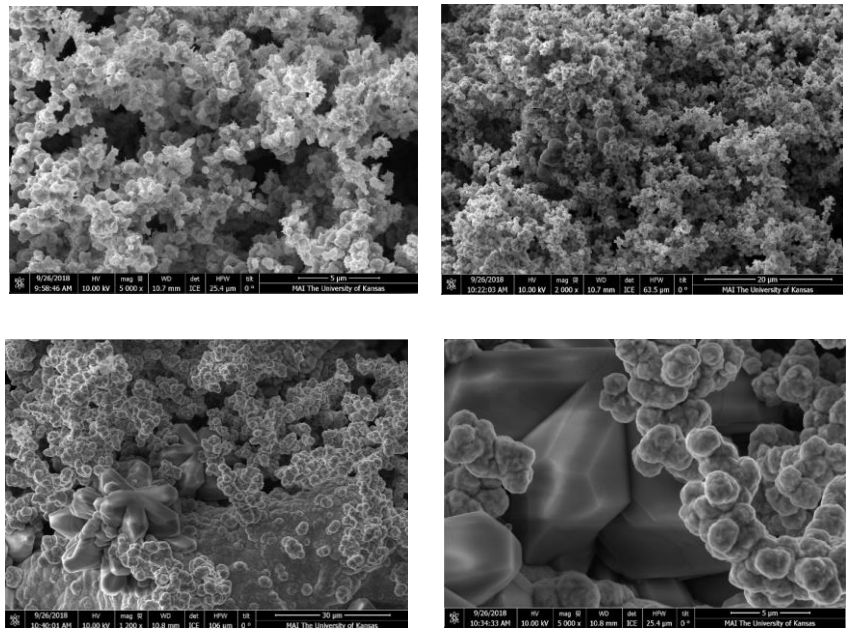

Figure 3.5: SEM images of Co_3S_4 at different magnifications.

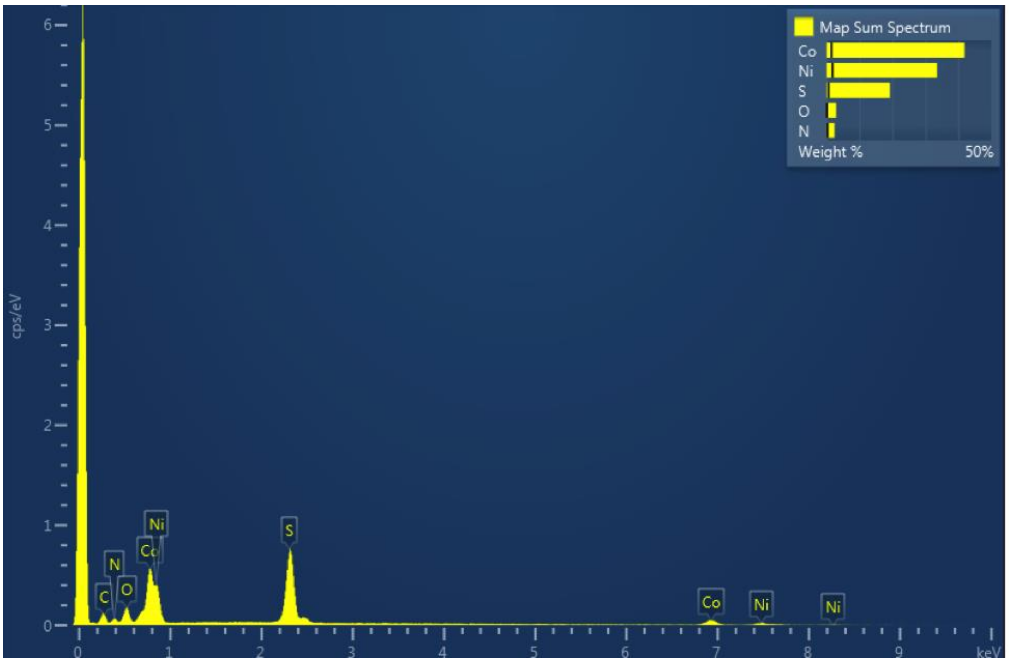

Figure 3.6: EDX spectrum of Co_9S_8 sample.

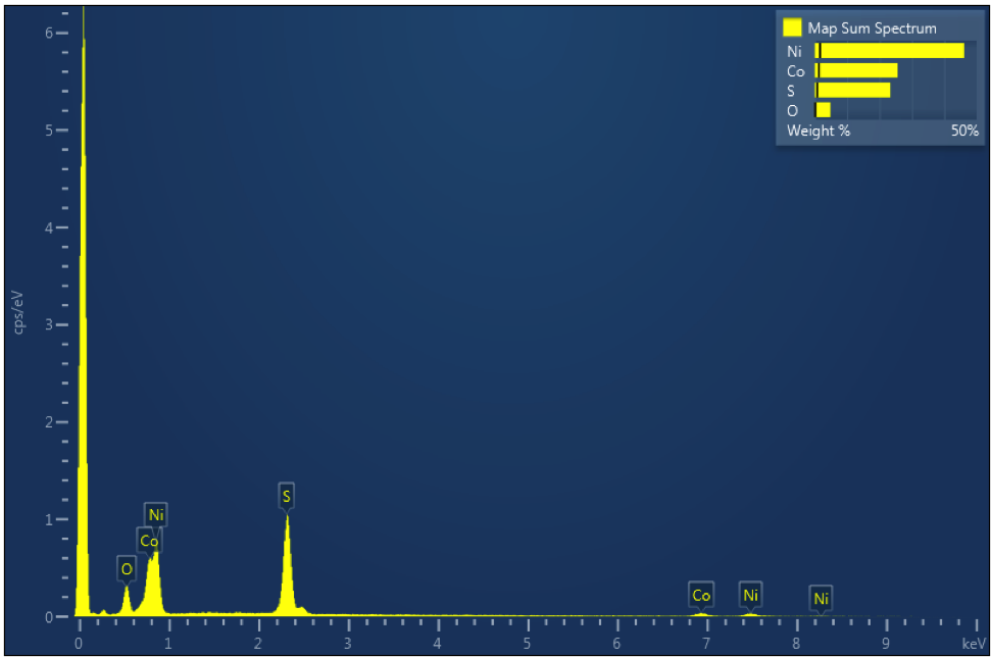

Figure 3.7: EDX spectrum of Co_3S_4 sample.

3.1.3: X-ray photoelectron spectroscopy:

X-ray photoelectron spectroscopy was utilized to investigate electronic and chemical composition of cobalt sulfides as-synthesized at low and high resolution spectrum. Figure 3.8 and Figure 3.9 display survey scan spectrum of Co_9S_8 and Co_3S_4. The presence of Co, S, elements in nanostructure of Co_9S_8 and Co_3S_4 can be clearly seen, while the strong peak of C 1s and O 1s is seen at 284.6 eV and 532. eV respectively could be from ambient environment. At high resolution, there are two peaks at 796.7 eV and 781.4 eV corresponding to Co $2p_{½}$ and Co $2p_{3/2}$ atomic orbitals (Figure 3.10 and Figure 3.11). These two peaks appearing in both Co_9S_4 and Co_3S_4 confirming the presence of Co^{2+} and Co^{3+}.[35,36] The S 2p peaks at 161.6 eV and 163.7 eV match well with S $2p_{3/2}$ and S $2p_{1/2}$ of S^{2-}as displayed in Figures 3.14 and 3.15.[37] Figure 3.12 and Figure 3.13 show a small amount of oxygen in both Co_9S_8 and Co_3S_4 with the peak located at 531.9, which corresponding to O 1s orbital.[38] According to the quantitative analysis of XPS, the atomic ratio of Co/S in Co_9S_8 and Co_3S_4 is determined to be 1.38 and 0.68 respectively, which is quite close to theoretical reports. Therefore, excellent electrochemical properties are expected.

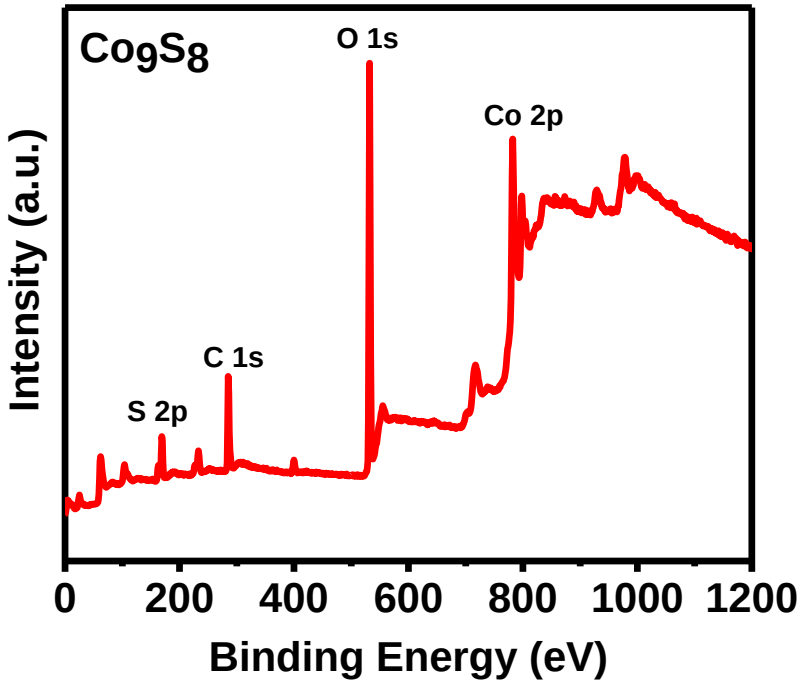

Figure 3.8: XPS survey scan spectrum of Co_9S_8.

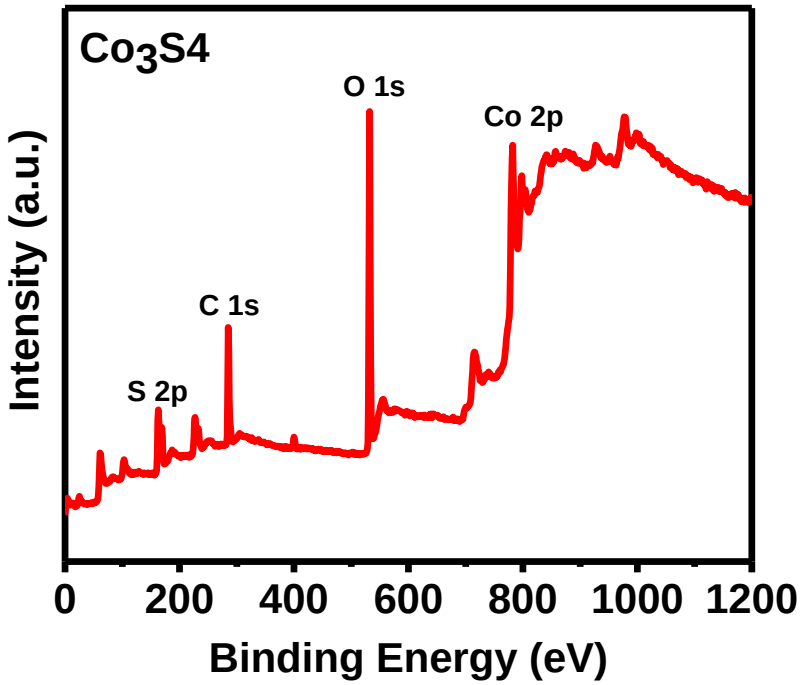

Figure 3.9: XPS survey scan spectrum of Co_3S_4.

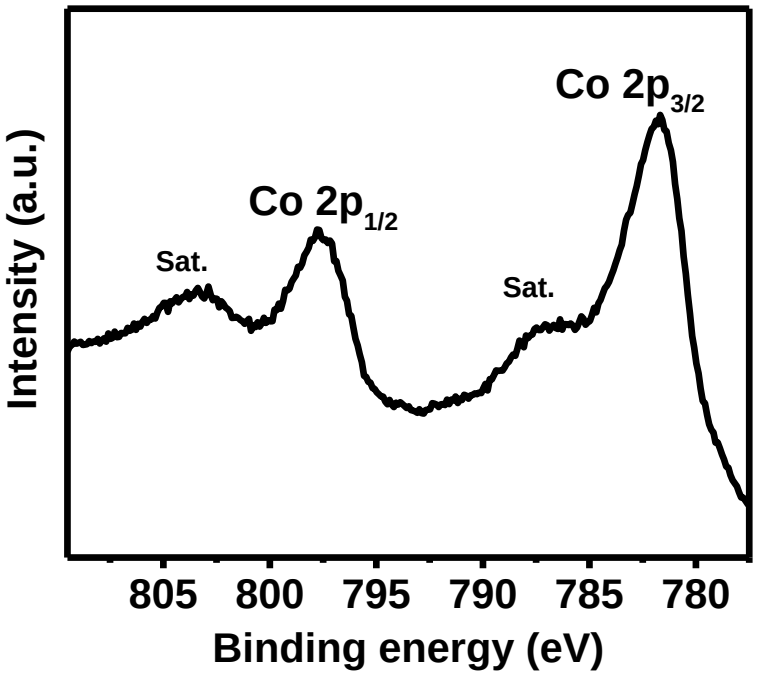

Figure 3.10: XPS spectra of Co 2p for Co_9S_8.

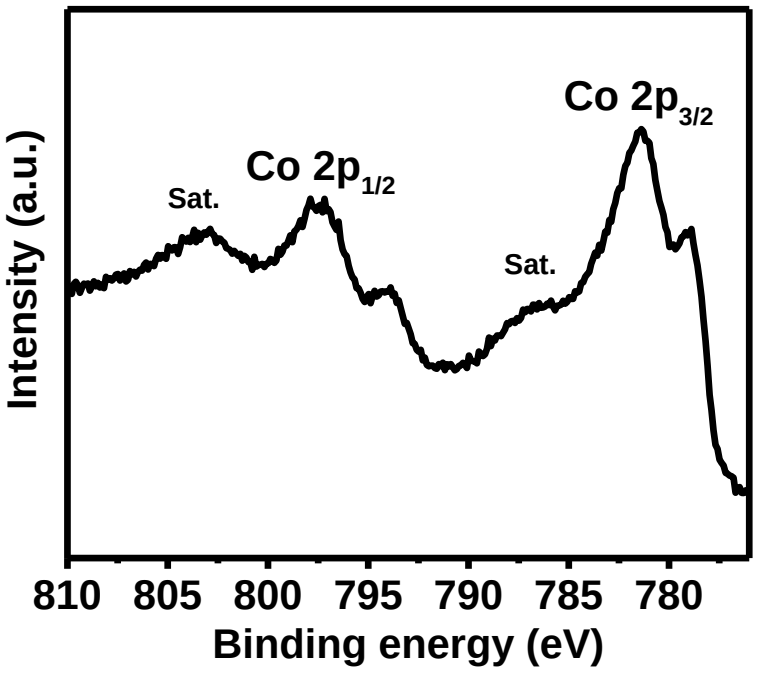

Figure 3.11: XPS spectra of Co 2p for Co_3S_4.

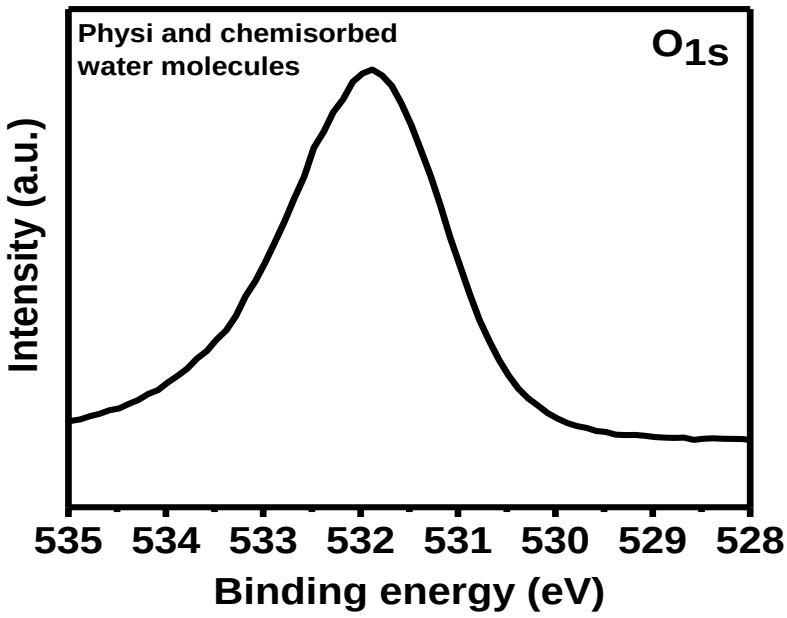

Figure 3.12: XPS spectra of O 1s for Co_9S_8.

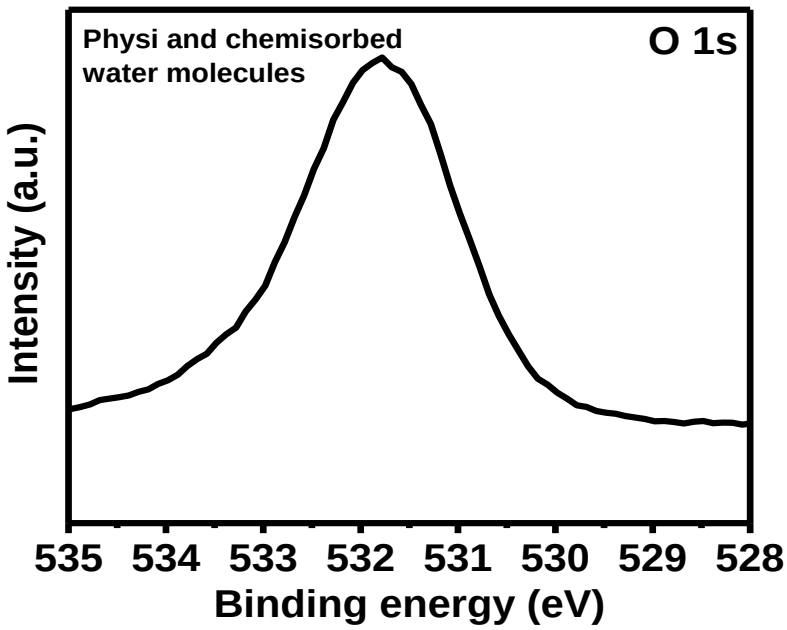

Figure 3.13: XPS spectra of O 1s for Co_3S_4.

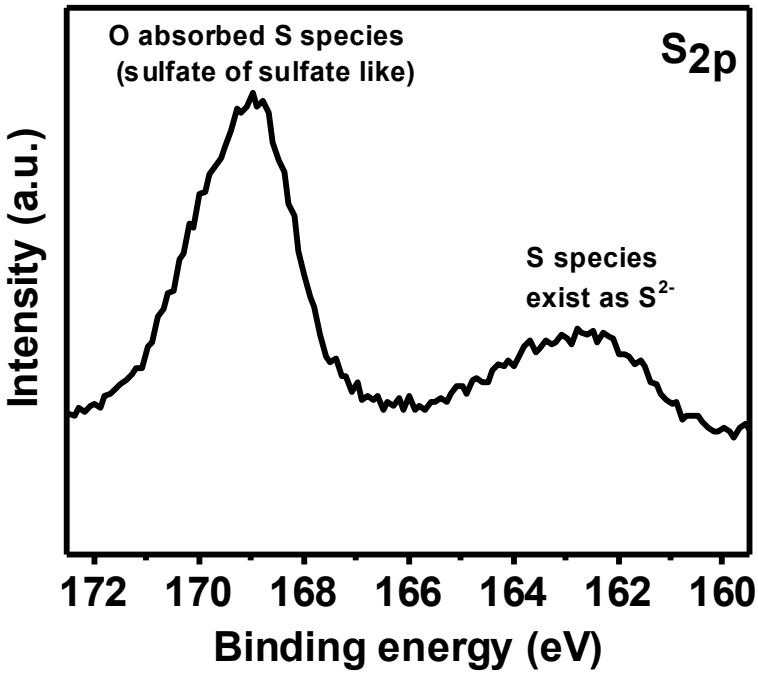

Figure 3.14: XPS spectra of S 2p for Co_9S_8.

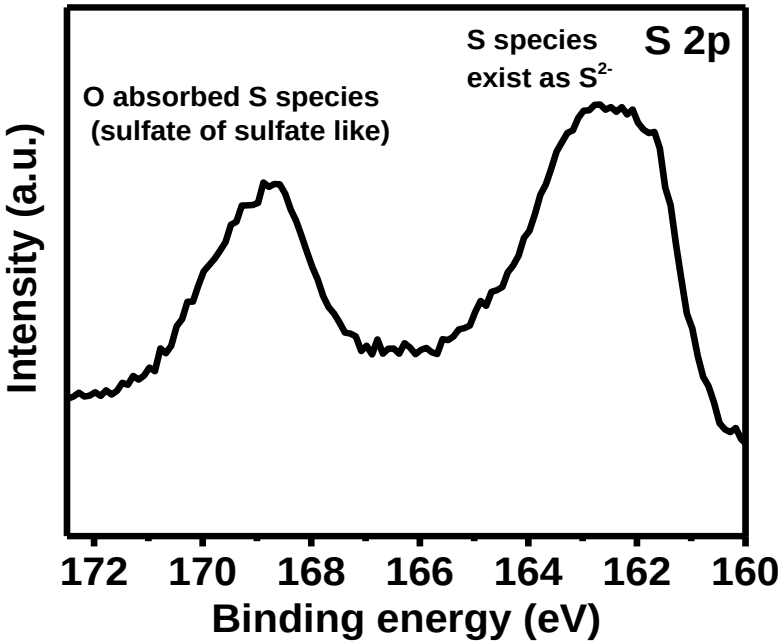

Figure 3.15: XPS spectra of S 2p for Co_3S_4.

3.2 Electrochemical measurements for supercapacitors:

Electrochemical properties and potential application for supercapacitors were investigated in a three-electrode system with 3M as an electrolyte. The electrochemical measurements were done through cyclic voltammetry, Galvanostatic charge-discharge measurements and electrochemical impedance spectroscopy.

3.2.1 Cyclic voltammetry:

Electroanalyses of cyclic voltammetry were performed to scrutinize the electrochemical behavior of the samples synthesized. Figures 3.16-3.20, show the CV curves of the samples synthesized at different scan rates (10 mV- 300 mV). It can be clearly seen although at high scan rates, the CV curves are symmetrical indicating a great outstanding stability of materials synthesized .[32-39] Furthermore, the CV curves were distinct with a pair of redox peaks. The cathodic peaks shift toward negative potential and the anodic peaks shift toward positive potential confirming quasi-reversible faradic reaction.

All faradic reactions of the synthesized materials in 3M KOH are shown below[55,56,57,58]:

$$Co(OH)_2 + OH^- \rightleftharpoons CoOOH + H_2O + e^- \ldots\ldots (4)$$

$$CoOOH + OH^- \rightleftharpoons CoO_2 + H_2O + e^-$$
$$Co_3O_4 + H2O + OH^- \rightleftharpoons 3CoOOH + e^- \ldots.. (5)$$

$$Co_9S_8 + 9OH^- \rightleftharpoons Co_9S_8(OH)_9 + 9e^- \ldots.. (6)$$

$$Co_3S_4 + OH \rightleftharpoons 4Co_3S_4OH^- + e^-$$
$$Co_3S_4OH^- + OH^- \rightleftharpoons 4Co_3S_4O + H_2O + e^- \ldots\ldots (7)$$

Also, there is a large area to the current and voltage plot, indicating high charge

storage due to the high surface area of the electrode prepared.[40-41] Specifically, more narrow peaks were observed in Figure 3.19, which can be attributed to faster redox reaction.[41]

To verify the specific capacitance of the materials synthesized, cyclic voltammetry was used to calculate the specific capacitance based on the following expression[41]:

$(Csp) = Q/(\Delta V \times A)$ …. (8)

Where Q is the area under the CV curve, ΔV is the potential window, and A is the area of the synthesized sample used in the electrode.[42] The distinction of the specific capacitance as a function of scan rate for all the synthesized samples of cobalt-based materials is shown in Figure 3.20. As shown in Figure 3.20, the specific capacitance has decreased with increased scan rates for all synthesized samples. It is notable to mention that at high scan rates, an electrolyte has sufficient time to diffuse only to the external surface of the active electrode which causes decreased capacitance. In contrast, at low scan rates the electrolyte has enough time to diffuse efficiently into most surface area of the electrode. Hence, the inner surface area has the highest contribution to the capacitance.[43-44-40] Table 3.1 shows the specific capacitance of all synthesized cobalt-based materials at a scan rate of 2 mV/s scan rate. A specific capacitance of 12,751 mF/cm^2 was obtained for Co_3S_4. Co_3S_4 shows the highest specific capacitance in comparison to Co_3O_4, $Co(OH)_2$ and Co_9S_8.

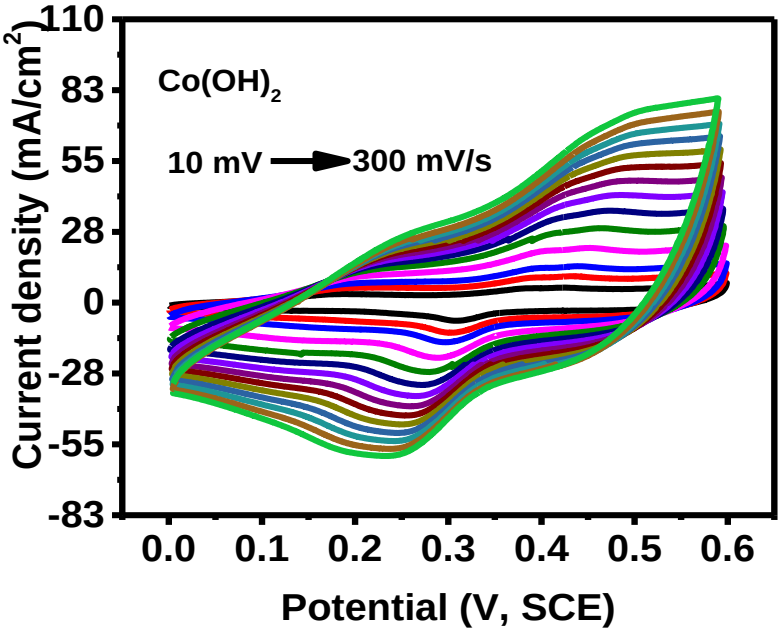

Figure 3.16: Cyclic voltammograms of $Co(OH)_2$ sample at various scan rates.

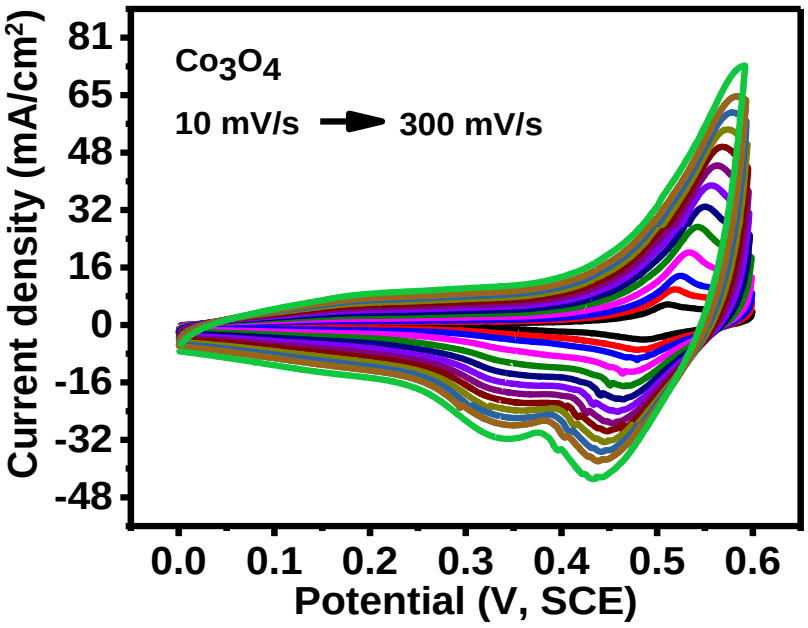

Figure 3.17: Cyclic voltammograms of Co_3O_4 sample at various scan rates.

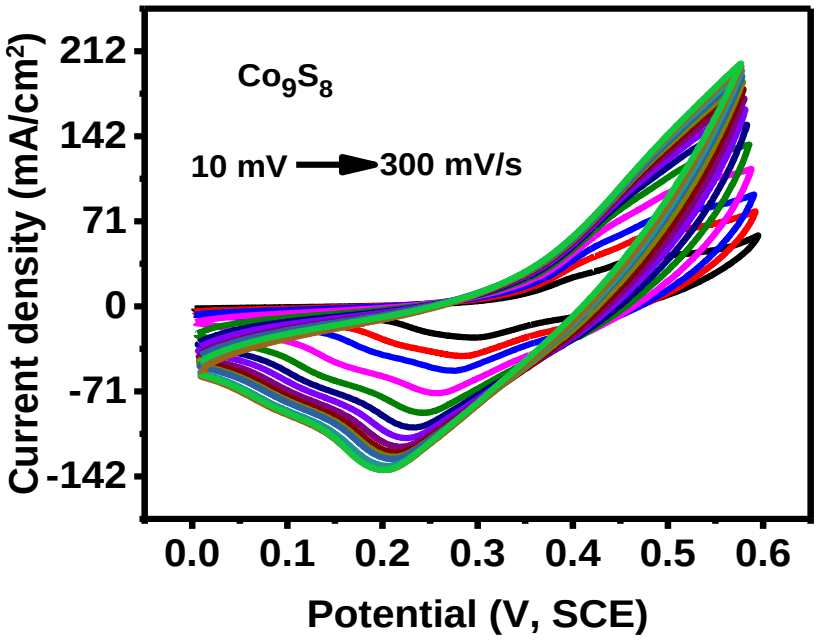

Figure 3.18: Cyclic voltammograms of Co_9S_8 sample at various scan rates.

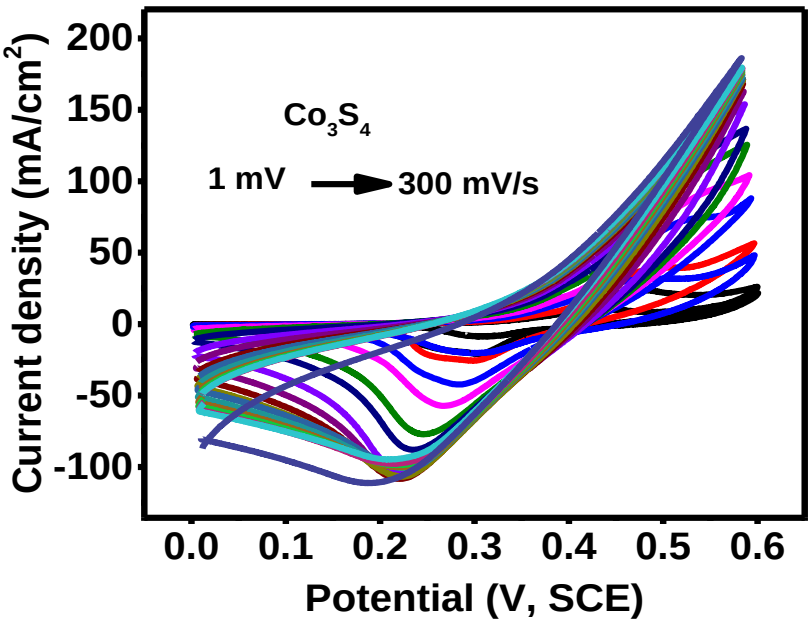

Figure 3.19: Cyclic voltammograms of Co_3S_4 sample at various scan rates.

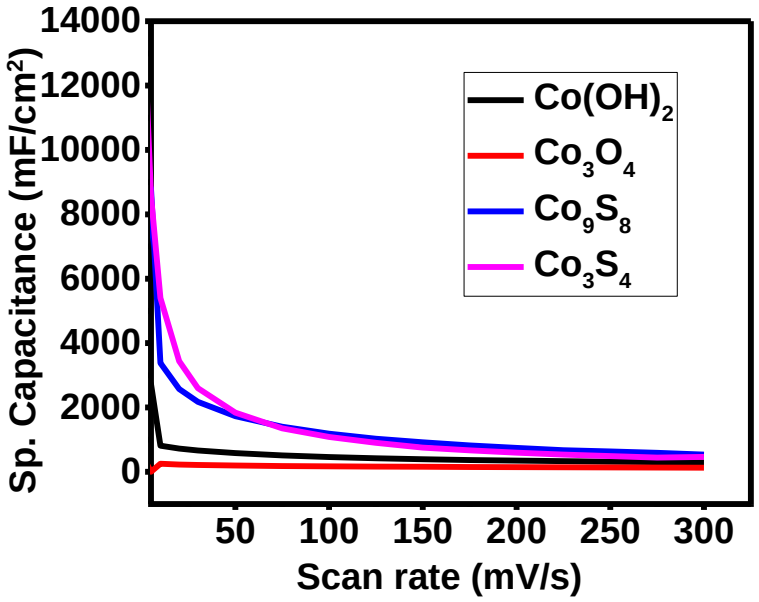

Figure 3.20: Variation of specific capacitance as a function of scan rates for all synthesized samples of cobalt-based materials in 3M KOH electrolyte.

Table 3.1: Specific capacitance of all the synthesized materials at 2 mV/s.

Sample code	Specific capacitance (mF/cm^2)
$Co(OH)_2$	1093
Co_3O_4	335
Co_9S_8	6172
Co_3S_4	12751

3.2.2 Galvanostatic charge-discharge:

To further investigate electrochemical properties for cobalt-based materials, Galvanostatic charge- discharge measurement was performed at different current densities in potential range (0-0.6 V). The charge-discharge mechanism of the cobalt-based materials electrodes are shown in Figures 3.21- 3.24. As illustrated in these figures, all samples showed highly symmetric nonlinear charge-discharge, recording the superior redox reaction reversibility and confirming the pseudo-capacitive characteristics of the electrodes. These pseudo-capacitive characteristics resulted because of charge-transfer reaction and the electrochemical adsorption-desorption process.[45-46] In addition, it was observed that the discharge time decreased with increasing current density, which could be due to the lack of electrolyte mobility to execute redox reaction at the electrode-electrolyte interface. Moreover, it was observed that the discharge time increased with an increase in the ratio of sulfide in the synthesized Co_9S_8 and Co_3S_4, thus enhancing the charge storage capacity. Galvanostatic charge-discharge measurements were used to calculate the specific capacitance of synthesized electrodes based on the following equation[47]:

$C_{sp} = (I/cm^2 \times \Delta t)/ \Delta V$….(9)

Where C*sp* is the specific capacitance in (mF/cm^2), I/cm^2 is the current density (mA/cm^2), Δ t is the discharge time (s), and ΔV is the potential window (V). Figure 3.25 shows the variations in the specific capacitance versus the current densities. As documented, Co_3S_4 has the highest specific capacitance of 8,508 mF/cm^2 among synthesized electrodes, whereas the specific capacitance of Co_9S_8, $Co(OH)_2$ and Co_3O_4 were 2470 mF/cm^2, 334 mF/cm^2 and 103 mF/cm^2 respectively as shown in Table 3.2.

Table 3.2: Specific capacitance of all the synthesized materials.

Sample code	Specific capacitance (mF/cm^2)
$Co(OH)_2$	103
Co_3O_4	334
Co_9S_8	2470
Co_3S_4	8508

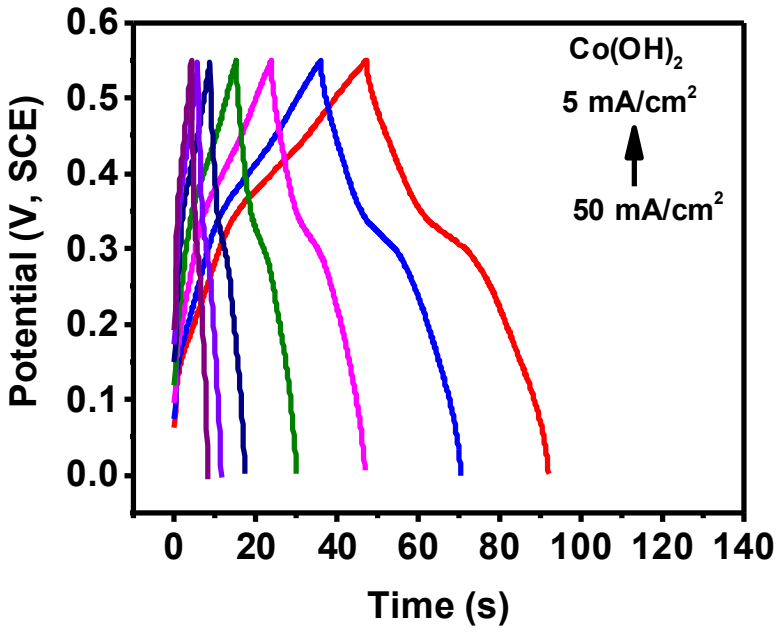

Figure 3.21: Galvanostatic charge-discharge curves of $Co(OH)_2$ at various current densities in 3M KOH.

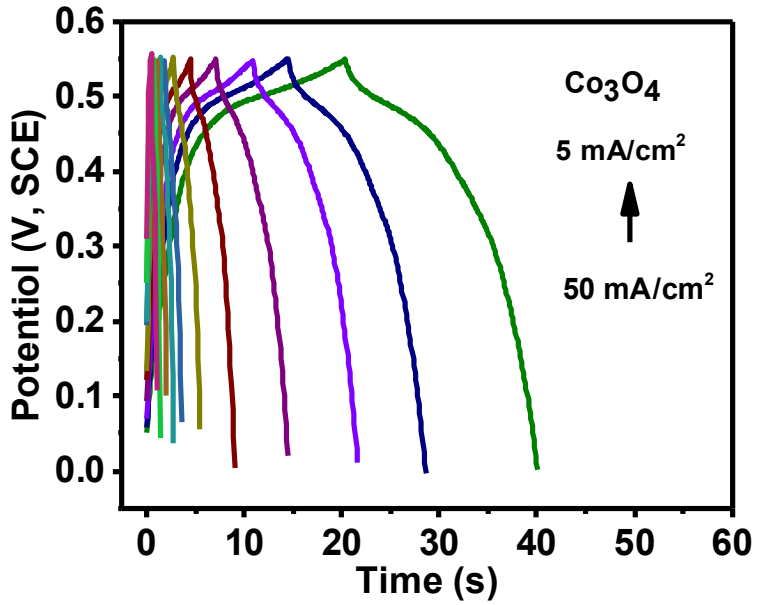

Figure 3.22: Galvanostatic charge-discharge curves of Co_3O_4 at various current densities in

3 M KOH

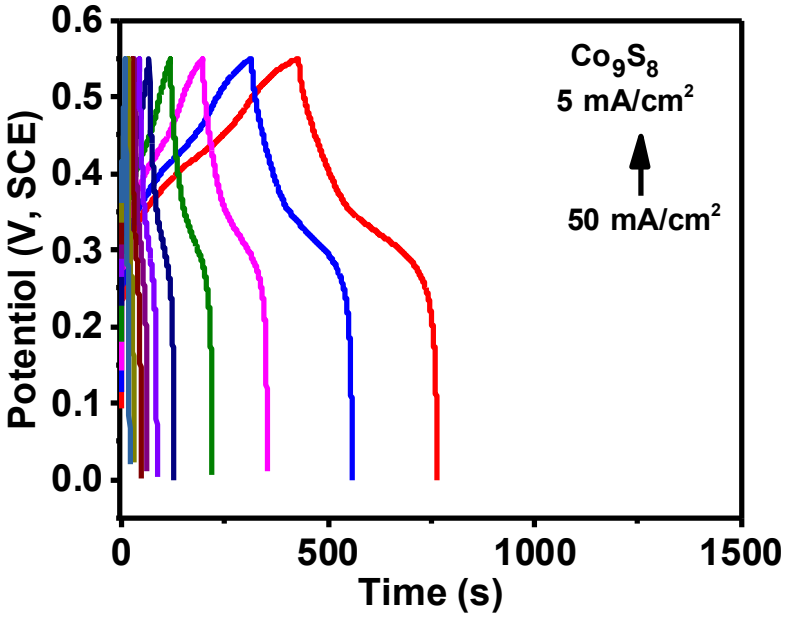

Figure 3.23: Galvanostatic charge-discharge curves of Co_9S_8 at various current densities in 3M KOH.

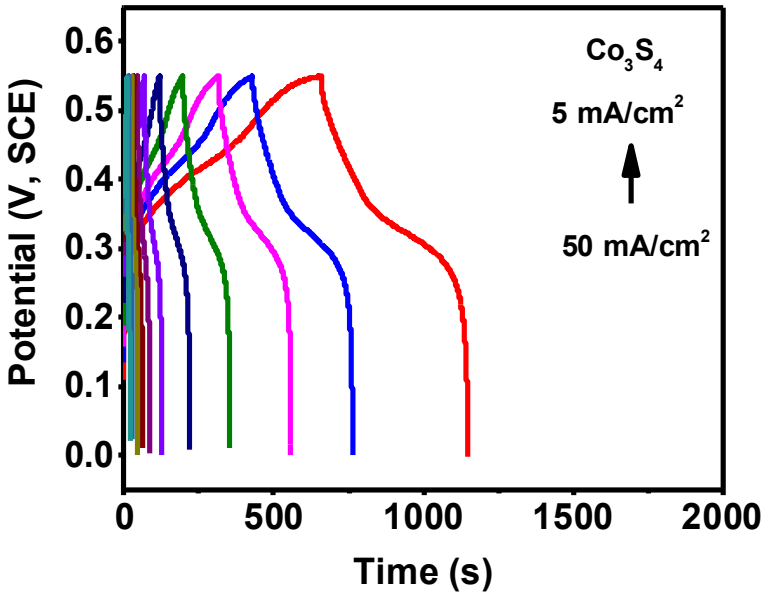

Figure 3.24: Galvanostatic charge-discharge curves of Co_3S_4 at various current densities in 3M KOH.

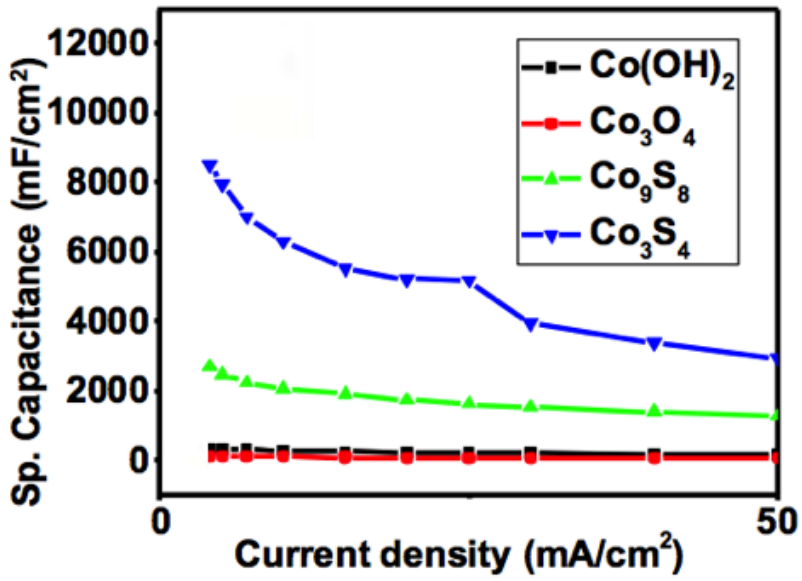

Figure 3.25: The variation of specific capacitance versus current densities for all synthesized samples in 3M KOH.

3.2.3 Electrochemical stability of synthesized electrode:

According to the above discussion, Co_3S_4 showed the highest specific capacitance, therefore the electrochemical cycle stability test and coulombic efficiency were further investigated for this electrode. The cyclic Galvanostatic charge-discharge approach was followed to study the capacitance retention versus the number of charge-discharge cycles as shown in Figure 3.26. The electrode possesses a life cycle stability of 120% retention of its initial capacitance over 5,000 cycles. The coulombic efficiency was also measured with a stable high value of 99%. Long-term life cycle and high coulombic efficiency are attributed to significant adequacy of Co_3S_4 as-prepared electrode.

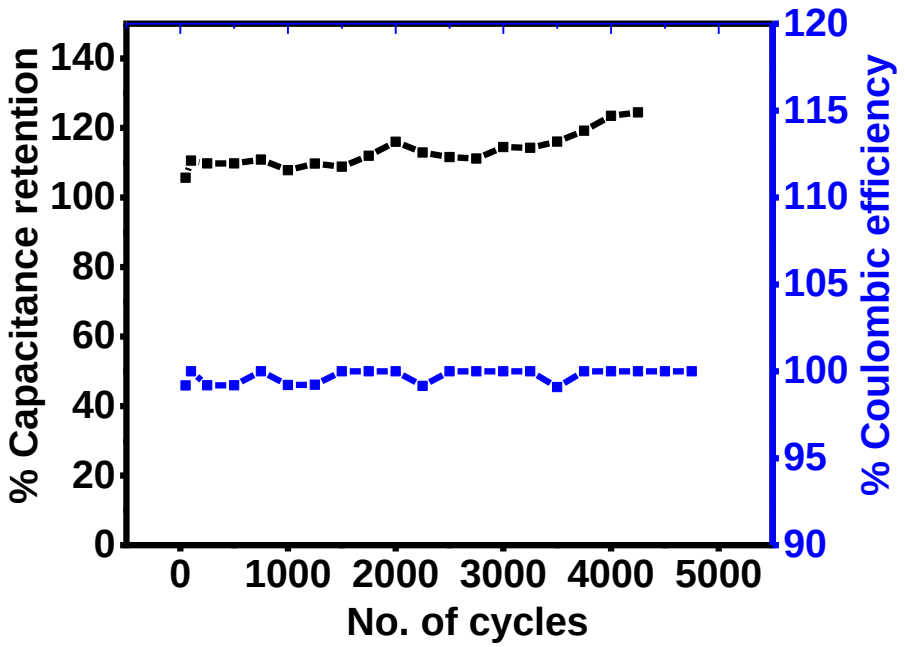

Figure 3.26: Cycling performance and coulombic efficiency of Co_3S_4.

3.3 Water splitting measurement

3.3.1 Oxygen evolution reaction:

Linear sweep voltammetry and electrochemical impedance spectroscopy were performed using three electrode system in 1M KOH alkaline media, to investigate the electrocatalytic property of synthesized materials for oxygen evolution reaction. As presented in the polarization curves in Figure 3.27, Co_3S_4 resulted in an overpotential of 126 mV to achieve OER at 10 mA/cm^2, surpassing those of Co_3O_4 (384 mV), $Co(OH)_2$ (336 mV), and Co_9S_8 (251 mV) as shown in Table 3.3, pointing out excellent performance of Co3S4 for OER activity. However, the obtained electrode of Co_3S_4 was observed to have high current densities. Tafel slope was investigated for all synthesized electrodes to study the kinetic transfer of the electrons through OER mechanism. Tafel slope was calculated based on the equation[49]:

$$\eta = b \log j + c \quad \ldots\ldots(10)$$

Where j is the current density, b is the slope, η is the overpotential, and c is a constant. The value of Tafel slope (b) is highly controlled by the kinetics of OER, so that lower Tafel slope indicates the faster kinetic of OER.[49] As seen in Figure 3.28, Co_3O_4 synthesized electrode showed the lowest Tafel slope of 51 mV/dec.

Moreover, electrochemical impedance spectroscopy was also performed to analyze and evaluate the electrocatalytic activity of synthesized electrodes. Figure 3.29 illustrates the impedance as a function of frequency at 0.50 V vs. Hg/Hg_2Cl_2. As seen in this figure, Co_3S_4 has the lowest impedance, which shows high charge transport between the electrolyte and the active electrode indicating faster electrochemical reaction. Further evidence of charge transport

resistance as determined by the Nyquist plot as shown in Figure 3.30. Co_3S_4 is capable of charge transport among others samples as its charge resistance is the lowest one.[50] Figures 3.31 and Figure 3.32 demonstrate the electrochemical impedance spectra for Co_3S_4 at various potentials. It can be clearly seen in these figures that the total impedance decreases with the increased potential. Cyclic voltammetry in non-faradic region was used to determine the electrochemical active surface area in potential range of 0-0.6 V (vs. RHE), where no faradic reaction was observed. As seen in Figure 3.37, CV curves were studied at different scan rates to record the electrochemical double layer capacitance (C_{dl}). The slope value of Co_9S_8 and Co_3S_4 were calculated to be 7.01×10^{-4} mC/cm^2 and 2.08×10^{-3} mC/cm^2, respectively. This result indicates that Co_3S_4 has better effective surface area than Co_9S_8, which is directly proportional to the value of the electrochemical double layer capacitance, so the highest electrochemical active surface areas produce highest electrochemical property for both C_{dl} and water analyses.[48]

The long-term catalytic stability test for Co_3S_4 electrode was investigated by using linear sweep voltammetry, electrochemical impedance spectroscopy and chronoamperometry as presented in Figures 3.33-3.34. The LSV polarization curve of Co_3S_4 electrode remained stable and showed outstanding performance up to 1,000th cycle. LSV test confirmed that the Co_3S_4 revealed remarkable stability without any decay as an electroctalyst for OER.

The impedance as a function of frequency and the Nyquist plot for the electrode before and after the stability test at a potential of 0.5 V are tested in Figure 3.35 and Figure 3.36. The impedance stayed stable up to 1,000 cycles. Additionally, chronoamperometric measurement was done for further stability investigation of Co_3S_4 electrodes as shown in

Figure 3.37. A very small decay in current density was monitored, highlighting electrochemical stability of the Co_3S_4 electrode.

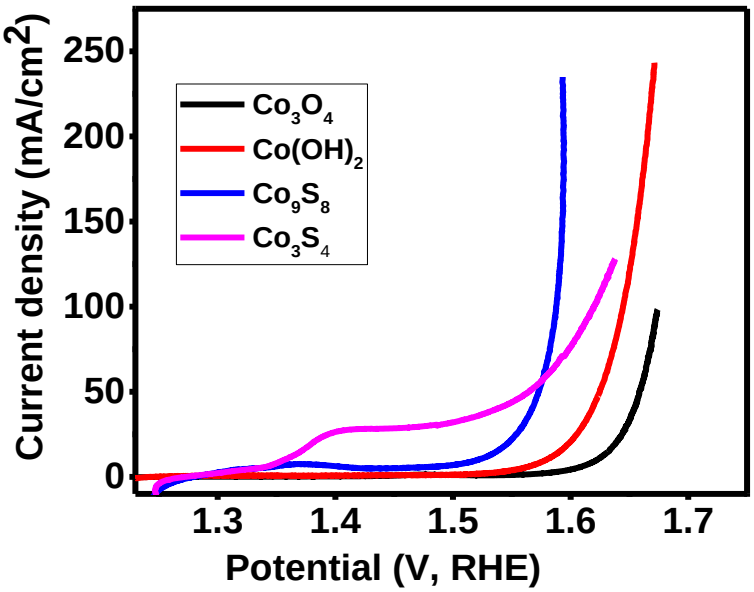

Figure 3.27: LSV polarization curves for all the synthesized samples.

Table 3.3: OER overpotential for all synthesized samples and corresponding Tafel slopes at 10 mA/cm2.

Samples	Overpotential (mV)	Tafel Slope(mV/dec)
$Co(OH)_2$	384	65
Co_3O_4	336	51
Co_9S_8	251	54
Co_3S_4	126	112

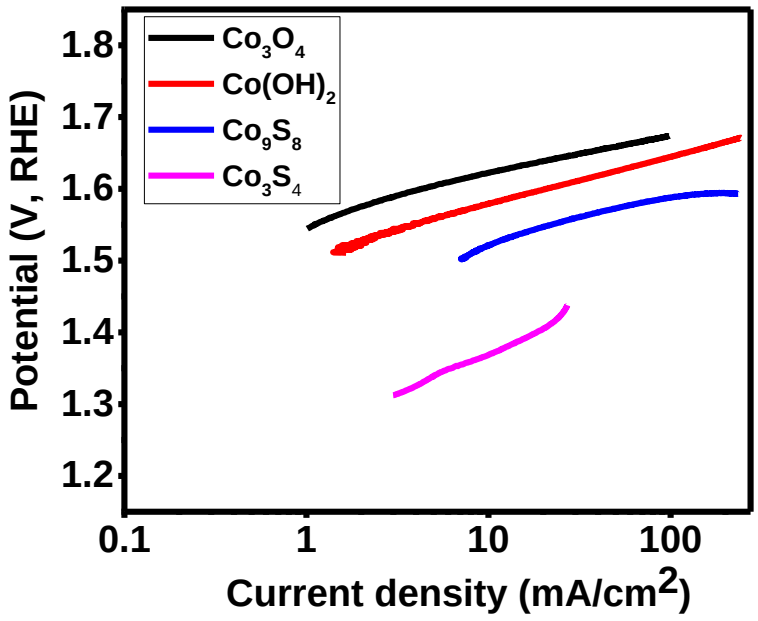

Figure 3.28: Tafel slopes for all the synthesized samples.

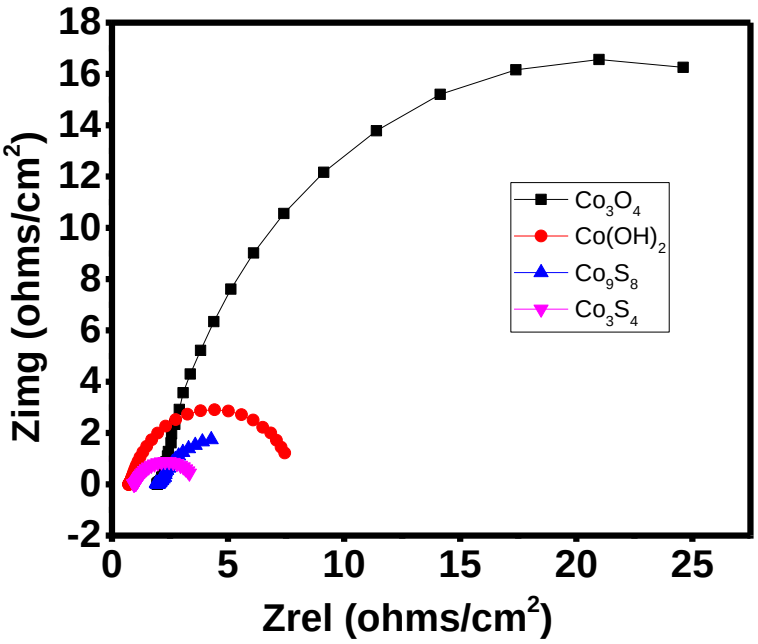

Figure 3.29: Nyquist plots of all the synthesized electrodes at 0.5 V vs. Hg/Hg_2Cl_2.

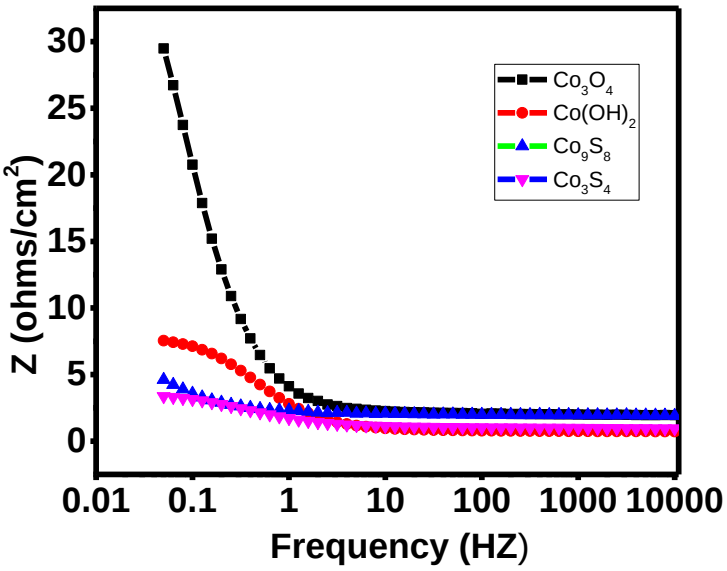

Figure 3.30: Impedance as a function of frequency for all the synthesized samples at 0.5 V vs. Hg/Hg_2Cl_2.

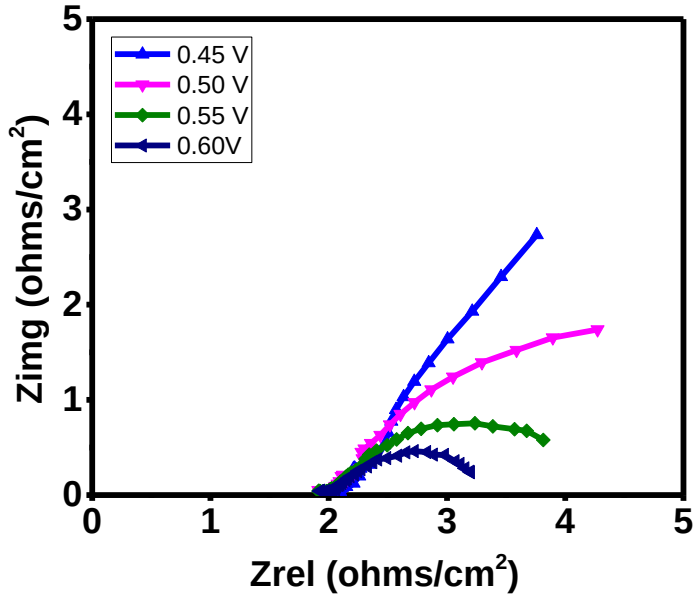

Figure 3.31: Variation Zre vs. Zim for Co_3S_4 sample at various voltages.

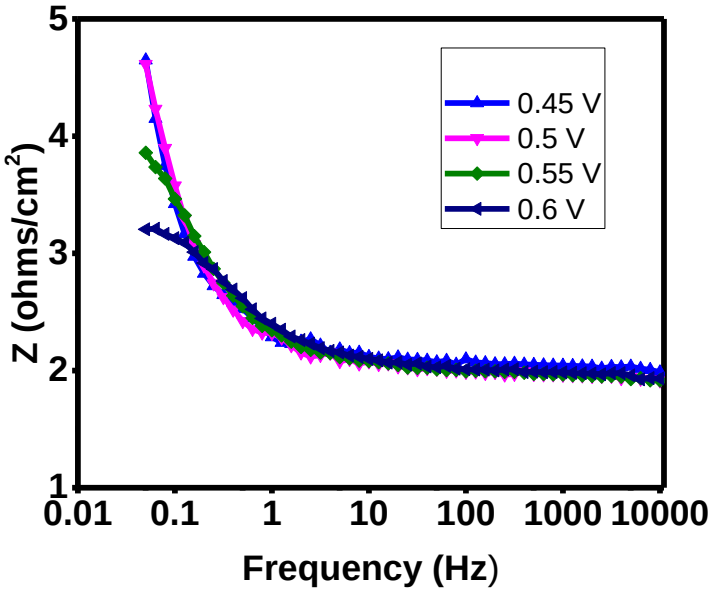

Figure 3.32: Variation of Z vs. frequency of Co_3S_4 at various voltages.

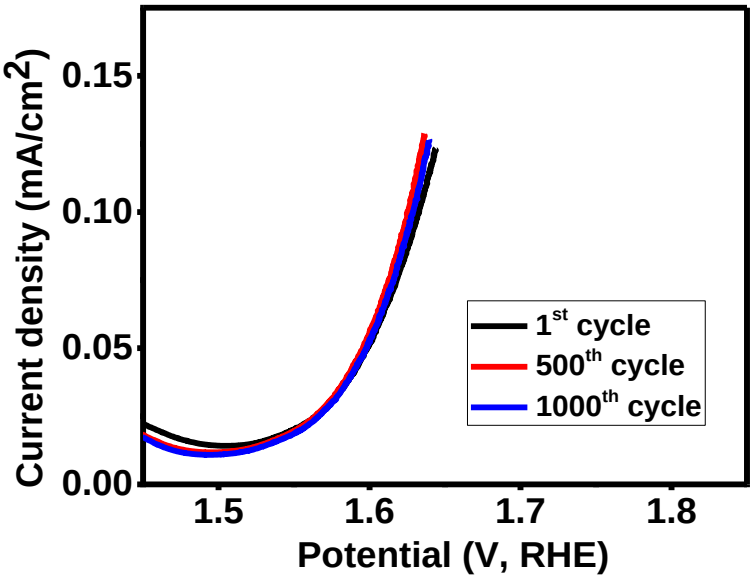

Figure 3.33: LSV polarization curves of Co_3S_4 at various cycles.

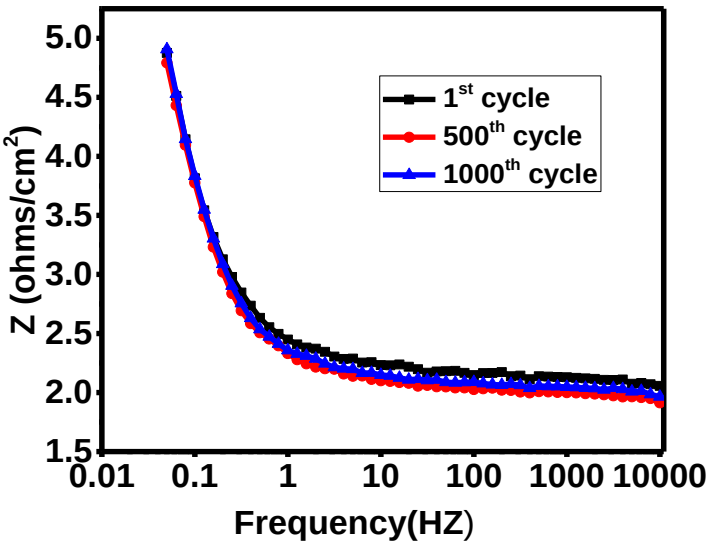

Figure 3.34: Impedance as a function of frequency plot of Co_3S_4 electrode at 0.5 V vs. Hg/Hg_2Cl_2 for the initial cycle, 500th cycle and the 1000th cycle.

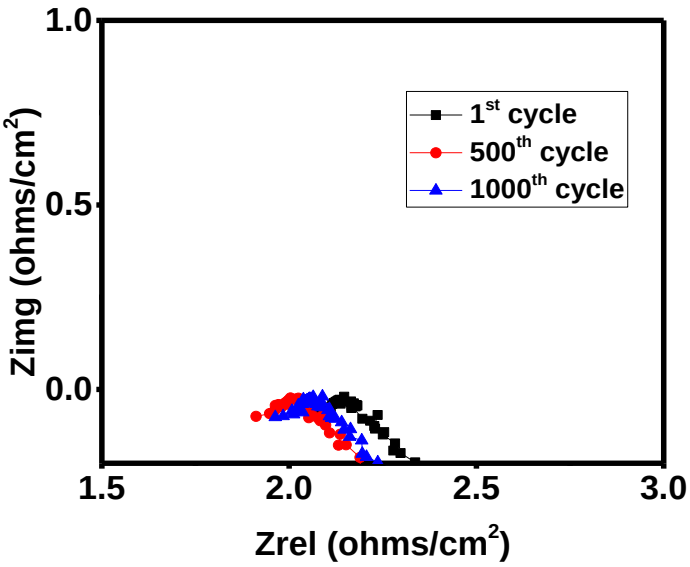

Figure 3.35: Nyquist plots of Co_3S_4 electrode at 0.5 V vs. Hg/Hg_2Cl_2 for the initial cycle, 500th cycle and the 1000th cycle.

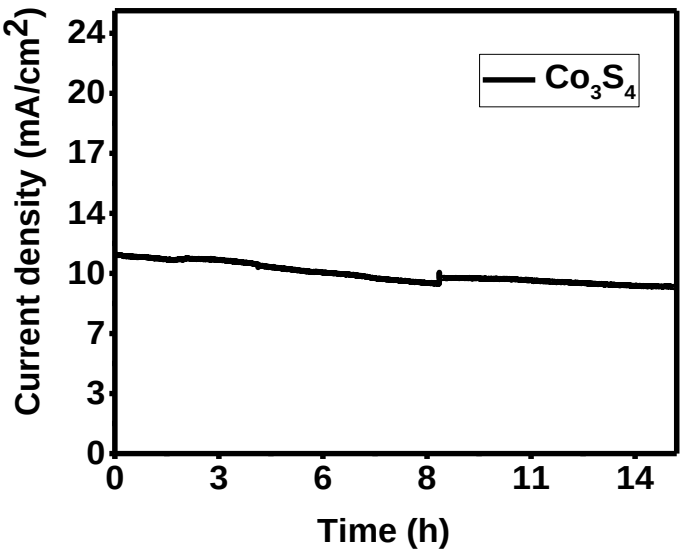

Figure 3.36: Time-dependent current density curve for Co_3S_4 synthesized electrode.

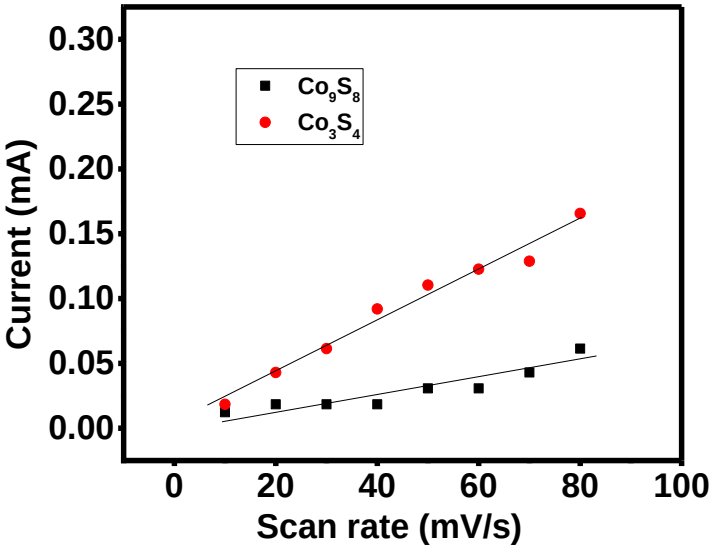

Figure 3.37: Difference of current vs. scan rate for Co_9S_8 and Co_3S_4.

3.3.2 Hydrogen evolution reaction:

Since water splitting consists of two half reactions, the OER at the anode and the HER at the cathode, hydrogen evaluation reaction was performed for all synthesized electrodes. Linear sweep voltammetry and electrochemical impedance spectroscopy were utilized to investigate the electrocatalytic behavior of all synthesized electrodes. As presented in Figure 3.38, different faces of cobalt sulfide Co_3S_4 and Co_9S_8 exhibited good HER-electro activity with lower overpotential of 217 mV to obtain a cathodic current density of 10 mA/cm^2, while other samples required 231 mV for Co_3O_4, $Co(OH)_2$ respectively. Table 3.4 corresponds to the overpotential for all synthesized samples at 10 mA/cm^2. Additionally, Tafel slope is shown in Figure 3.39.

Table 3.4: HER overpotential for all the synthesized samples at current density of 10 mA/cm^2.

Samples	Overpotential (mV)	Tafel Slope (mV/dec)
$Co(OH)_2$	231	59
Co_3O_4	231	48
Co_9S_8	217	43
Co_3S_4	217	48

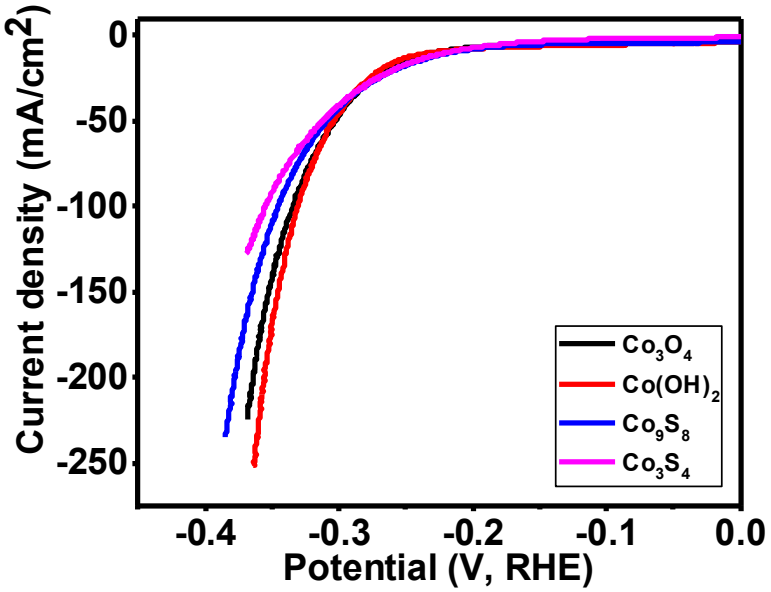

Figure 3.38: LSV polarization curves for all the samples.

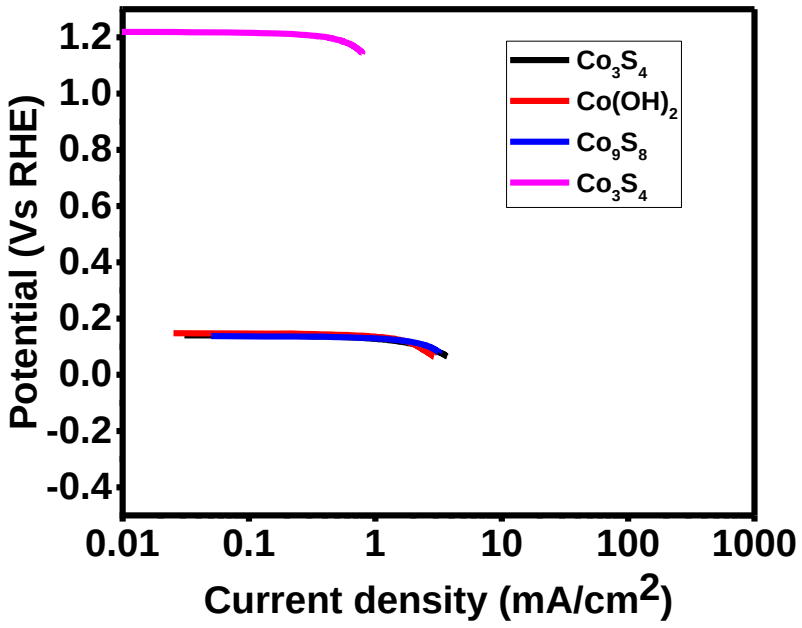

Figure 3.39: HER Tafel slopes for all the samples.

The electrical conducting behavior and HER activity of catalytic were verified by

using the electrochemical impedance spectroscopy measurements at -1.25 V vs. Hg/Hg_2Cl_2.It can be realized from Nyquist plot and Impedance as a function of frequency for all the synthesized electrodes in Figures 3.40-3.4 that Co_3S_4 displayed the lowest impedance among all synthesized samples which produced high electro-catalytic activity, clearly demonstrating faster charge transport through HER process.[51] To further investigate why Co_3S_4 exhibited high electrochemical performance in comparison with other samples, EIS measurements were conducted at different applied potential as well. Figures 3.42-3.43 show the charge transport behavior of Co_3S_4. As the resistance decreased, the potential increased, confirming better electrochemical reaction rates.[51-52]

As a substantial parameter to evaluate electrocatalysts, the stability of Co_3S_4 as a catalyst for HER was examined using linear sweep voltammetry. Figure 3.44 shows LSV polarization curves had stable overpotential up to 4000 cycles. To confirm, the impedance as a function of frequency and Nyquist plot for the catalytic before and after the stability test at a potential of -1.25 V were tested as shown in Figure 3.45 and Figure 3.46. There is a small fluctuation in Nyquist plot, while the impedance remains stable as shown in Figure 3.46. Furthermore, chronoamperometric measurements were also performed as shown in Figure 3.47. The current density remained constant over 16 hours. This result demonstrates the durability and efficiency of Co_3S_4 catalytic for HER.

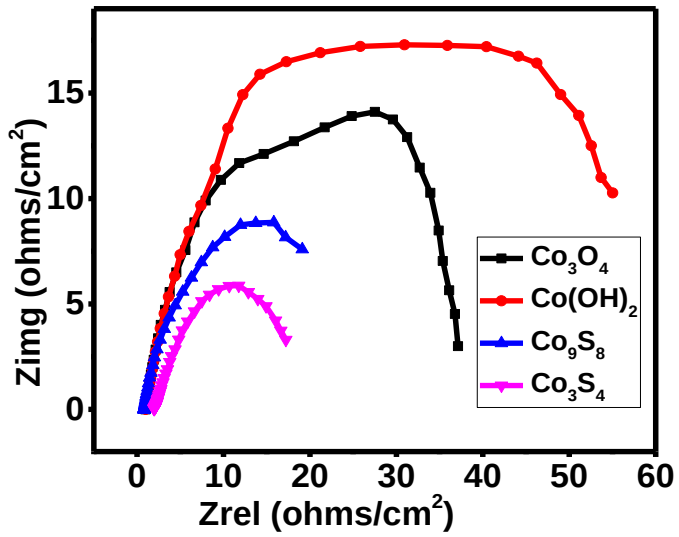

Figure 3.40: Nyquist plots of all the synthesized electrodes at -1.25 V vs. Hg/Hg_2Cl_2.

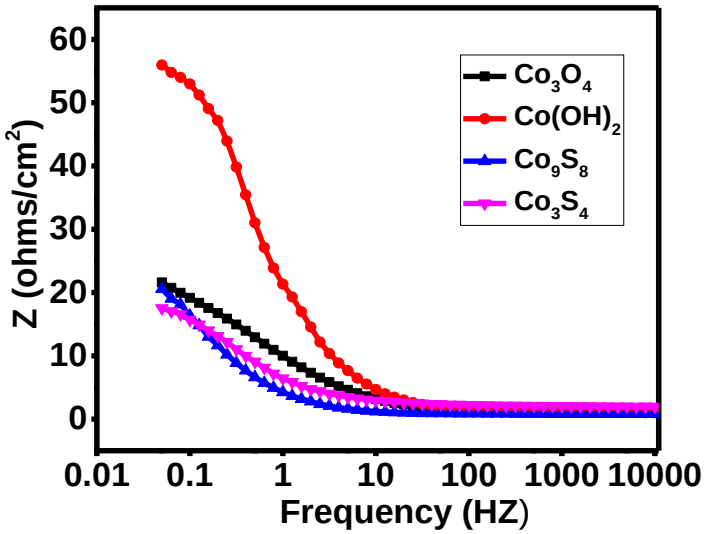

Figure 3.41: Impedance as a function of frequency for all the synthesized electrodes at -1.25 V vs. Hg/Hg_2Cl_2.

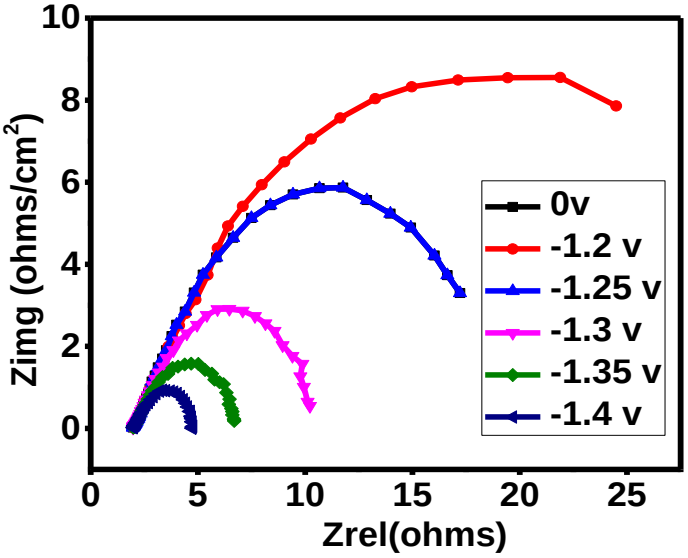

Figure 3.42: Nyquist plots of Co_3S_4 electrode at different potential.

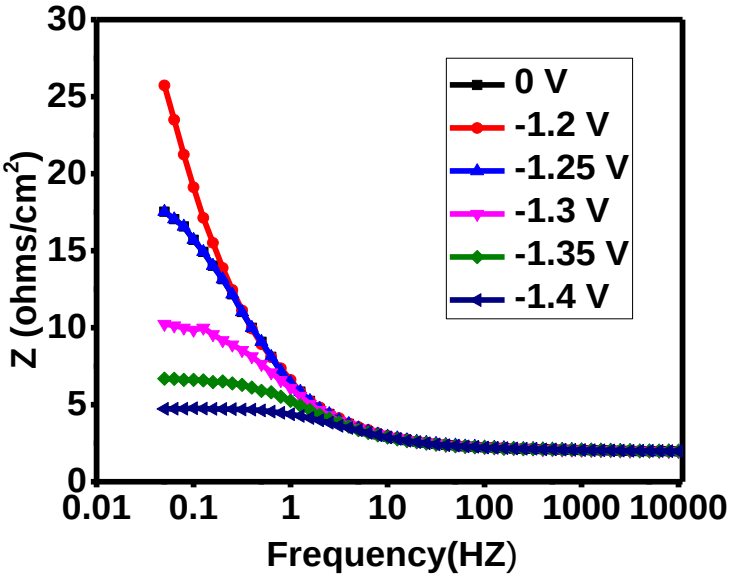

Figure 3.43: Impedance as a function of frequency plot of Co_3S_4 electrode at -1.25 V vs. Hg/Hg_2Cl_2.

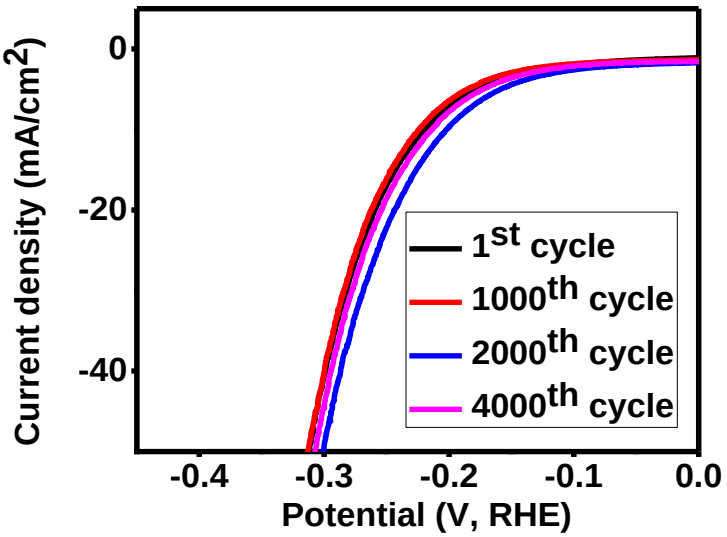

Figure 3.44: Polarization curves of Co_3S_4 at various cycles.

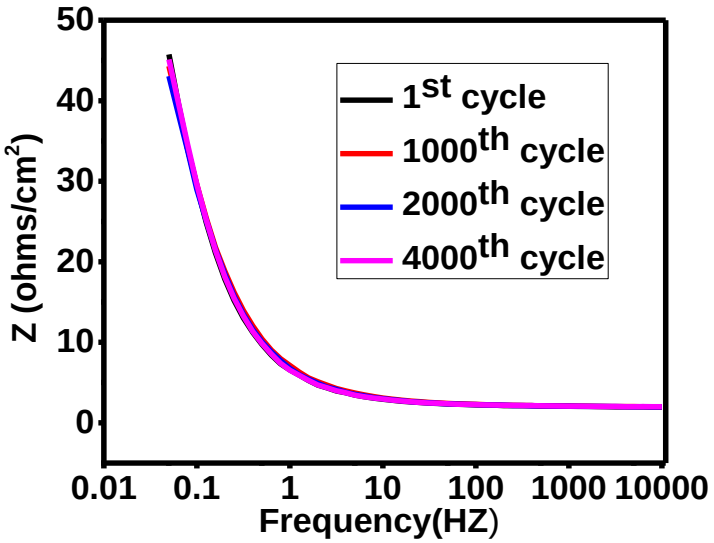

Figure 3.45: Impedance as a function of frequency plot of Co_3S_4 electrode at -1.25 V vs. Hg/Hg_2Cl_2 up to 4,000th cycles.

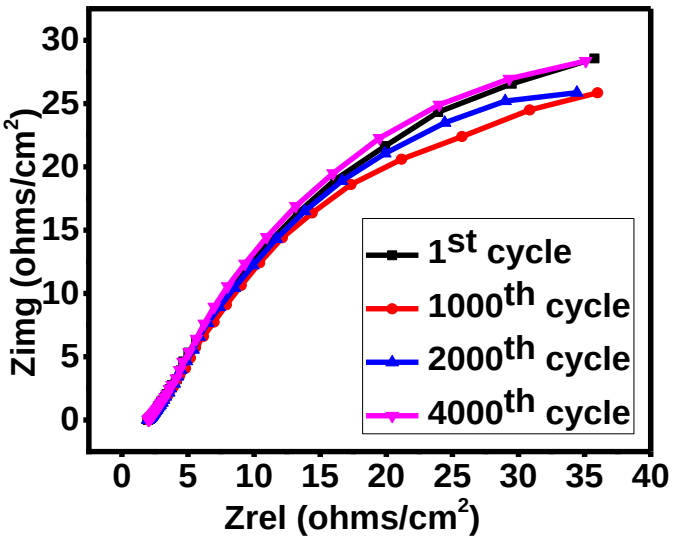

Figure 3.46: Nyquist plots of Co_3S_4 electrode at -1.25 V vs. Hg/Hg_2Cl_2 up to 4,000th cycles.

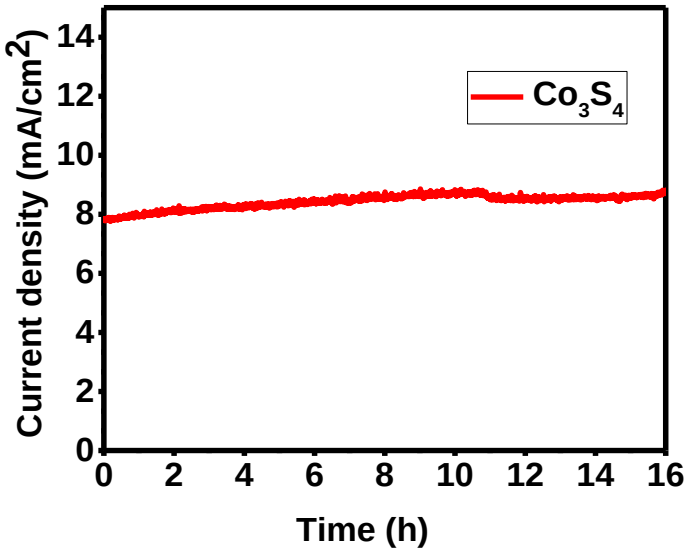

Figure 3.47: Electrochemical stability test of Co_3S_4 using chronoamperometry.

3.4. Overall water splitting:

An efficient and economical bifunctional electrocatalytic for both oxygen and hydrogen evolution reaction is still one of the essential challenges for overall water splitting. According to all documented results, the cobalt sulfide (Co_3S_4) exhibited highest electrochemical performance among synthesized electrodes. Therefore and perhaps, overall water-splitting measurements were driven in a two-electrode system using Co_3S_4 as an active catalytic for both the anodic and cathodic electrodes with 1M KOH alkaline solution as shown in Figure 3.48. Figure 3.49 recorded linear sweep voltammetry with capability of overall water potential 1.5 V at a current density of 10 mA/cm^2, which is much better than the benchmark catalysts of Pt and RuO_2,[53] confirming that the facile hydrothermal synthesis of Co_3S_4 is dominantly accountable for high activity of both OER and HER. To examine the charge transfer rate during the water splitting process, electrical impedance spectra was performed as shown in Figure 3.50 and Figure 3.51. As illustrated in these figures, the resistance of the solution is 5.02 ohm, highlighting high charge transform ability and conductivity. Figure 3.52 clarifies the chronoamperometric test. It can be clearly observed that current density was highly stable over 16 h, demonstrating that the Co_3S_4 offers an excellent overall water splitting performance with robust long-term stability.

The optimized performance of Co_3S_4 electrode could be attributed to its morphology and structure characterization with a mixture of nanospherical and multiple nanoflowers with octahedral edge facilitating the electrolyte to penetrate the entire surface area of the electrode.[54] So, from all the electrochemical measurements, it can be suggested

that Co_3S_4 could be utilized as a highly efficient and durable material for overall water splitting.

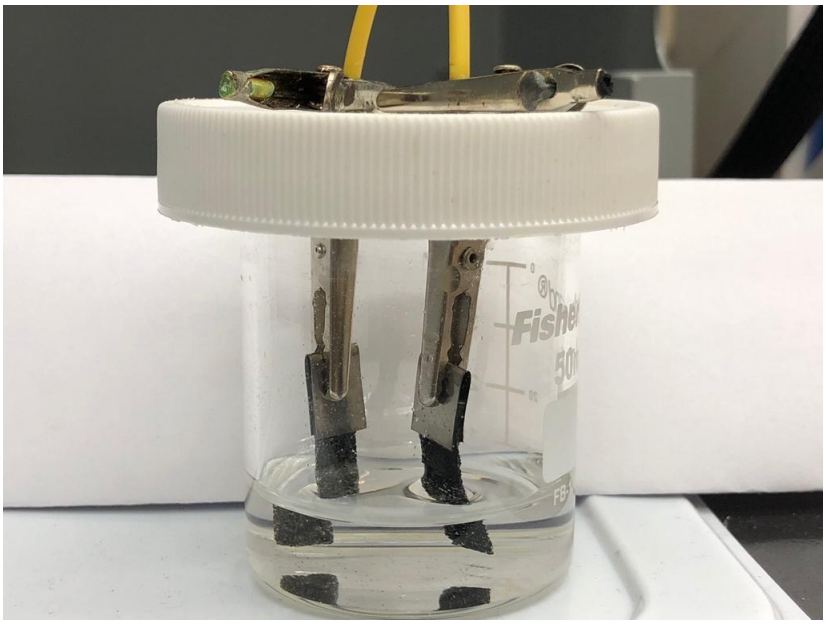

Figure 3.48: Scheme of water splitting cell.

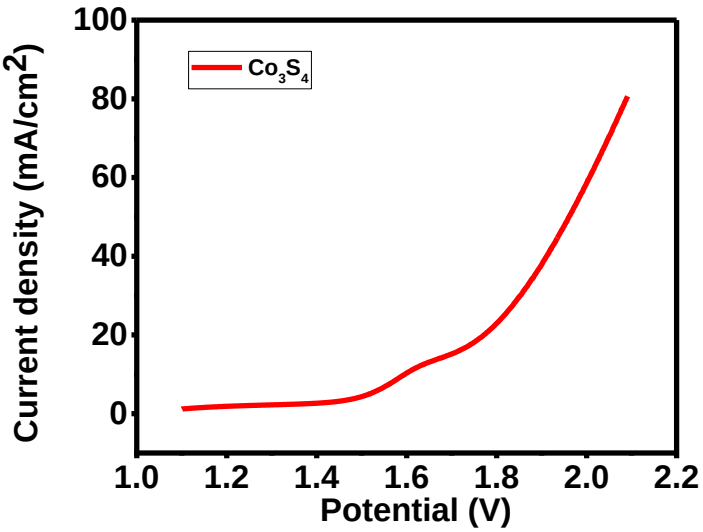

Figure 3.49: LSV for overall water splitting cell.

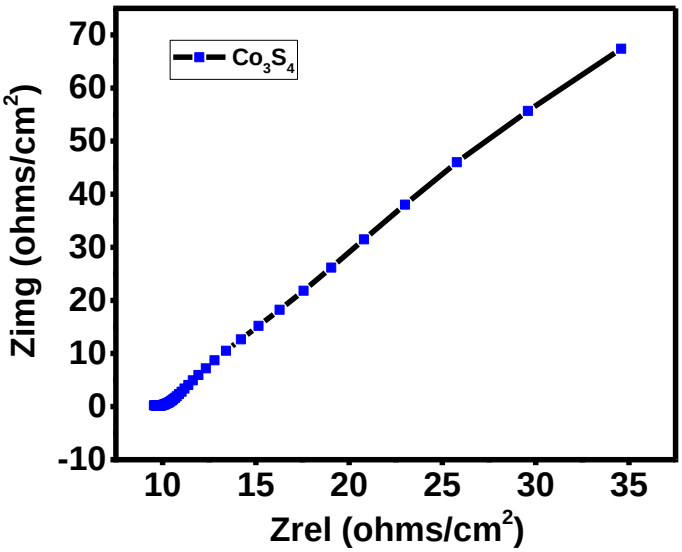

Figure 3.50: Nyquist plot of Co_3S_4 for water splitting cell.

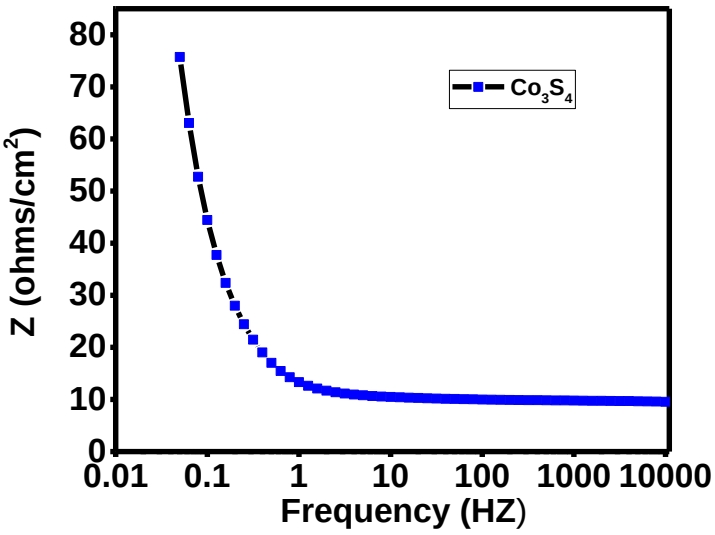

Figure 3.51: Impedance as a function of frequency plot of Co_3S_4 for overall water splitting.

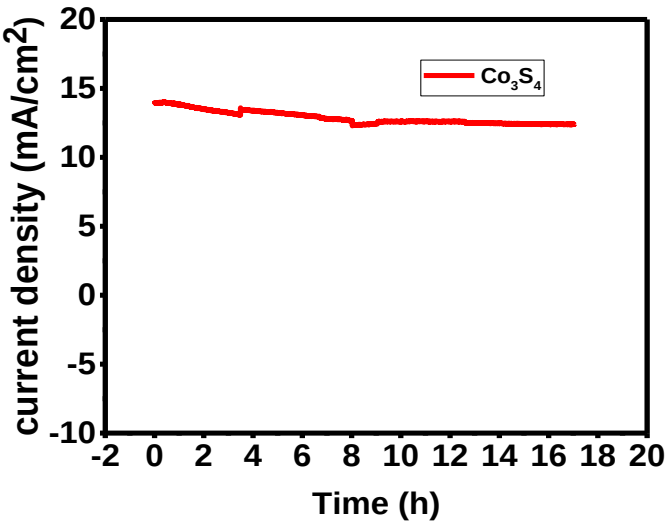

Figure 3.52: Time-dependent current density curves of Co_3S_4 for overall water splitting.

CHAPTER IV

CONCLUSION

In conclusion, multifunctional nanostructured cobalt-based materials were successfully synthesized by using a facile hydrothermal technique. The obtained characterization of the electrodes $Co(OH)_2$, Co_3O_4, Co_9S_8 and Co_3S_4 were performed utilizing several measurements. The phase purity and morphology were well defined using x-ray diffraction and scanning electron microscopy. The elemental composition was confirmed using an energy dispersive X-ray spectrometer. Electrochemical properties for all synthesized electrodes were studied in a three electrodes system. Cyclic voltammetry, galvanostatic charge-discharge, electrochemical impedance spectroscopy measurements and linear sweep voltammetry were performed to analyze the supercapacitance behavior of the synthesized electrodes and their potential for water splitting application.

The optimized results for charge storage capacity were recorded at 8508 mF/cm^2, 2470 mF/cm^2, 334 mF/cm^2 and 103 mF/cm^2 for Co_3S_4, Co_9S_8, $Co(OH)_2$ and Co_3O_4 respectively, which suggests that the mixture of nanospherical and multiple nanoflowers cobalt sulfide showed higher supercapacitance among synthesized electrodes with outstanding long-term life cycle stability of 120% retention of its initial capacitance over 5000 cycles. Our results suggest that multiple nanoflowers cobalt sulfide Co_3S_4 could be promising material for future supercapacitance devices.

Additionally, oxygen and hydrogen evolution reactions toward water splitting were evaluated in alkaline media. Co_3S_4 showed the lowest overpotential for both OER and HER with 126 mV and 217 mV respectively. Electrochemical stability of Co_3S_4 as an active catalyst was confirmed using chronoamperometric measurements. Furthermore, since Co_3S_4 was the best sample for OER and HER, overall water splitting was examined using a two electrode system. The same synthesized catalytic Co_3S_4 was used as cathodic and anodic electrodes. Overall water splitting was driven at very low cell overpotential of 1.5 V remaining stable over 16 h at 10 mA/cm^2.

The excellent electrochemical properties of synthesized nanostructured cobalt sulfide Co_3S_4 could be attributed to its nanostructure morphology, which is highly effective in maximizing the electrode activity. Our results suggest that multiple octahedral nanoflowers cobalt sulfide Co_3S_4 could be a promising multifunctional material for energy storage applications as well as energy generation.

References

(1) Tokbolat, S., Calay, R. K., & Al-Zubaidy, S. Renewable energy technologies and practices: Prospective for building integration in cold climates (Kazakhstan). *Journal of Renewable and Sustainable Energy*, 2015. *7*(5), 053124.

(2) Fraunhofer-Gesellschaft. Breakthrough in electricity storage: New large and powerful redox flow battery. *ScienceDaily*,2013.

(3) Larcher, D., & Tarascon, J. M. Towards greener and more sustainable batteries for electrical energy storage. *Nature chemistry*, 2015. *7*(1), 19.

(4) Alliance, G. M. The advantages and disadvantages of renewable energy, (2015).

(5) Will soutter.,What is an Ultracapacitor. *Azo Nano* ,2012.

(6) University of washngton. Supercapacitor. *clean energy institute*.

(7) Kim, B. K., Sy, S., Yu, A., & Zhang, J. Electrochemical supercapacitors for energy storage and conversion. *Handbook of Clean Energy Systems*, 2015, 1-25.

(8) Salunkhe, R. R.; Kaneti, Y. V.; Yamauchi, Y. Metal–Organic Framework-Derived Nanoporous Metal Oxides toward Supercapacitor Applications: Progress and Prospects. ACS Nano 2017, 11, 5293.

(9) Anantharaj, S., Ede, S. R., Sakthikumar, K., Karthick, K., Mishra, S., & Kundu, S. Recent trends and perspectives in electrochemical water splitting with an emphasis on sulfide, selenide, and phosphide catalysts of Fe, Co, and Ni: a review. *ACS Catalysis*,2016, *6*(12), 8069-8097.

(10) Bandal, H. A., Jadhav, A. R., Tamboli, A. H., & Kim, H. Bimetallic iron cobalt oxide self-supported on Ni-Foam: an efficient bifunctional electrocatalyst for oxygen and hydrogen evolution reaction. *Electrochimica Acta*, 2017,*249*, 253-262.

(11) Xu, P., Li, J., Luo, J., Wei, L., Zhang, D., Zhou, D., ... & Yuan, D. (Fe 0.2 Ni 0.8) 0.96 S tubular spheres supported on Ni foam as an efficient bifunctional electrocatalyst for overall water splitting. *Scientific reports*, 2018, *8*(1), 9425.

(12) Haniam, P., Kunsombat, C., Chiangga, S., & Songsasen, A. Synthesis of cobalt oxides thin films fractal structures by laser chemical vapor deposition. *The Scientific World Journal*, 2014.

(13) Yang, Q.; Lu, Z.; Sun, X.; Liu, J. Ultrathin Co3O4 Nano Sheet Arrays with High Supercapacitive Performance. Sci. Rep. 2013, 3, 1-7.

(14) Haniam, P.; Kunsombat, C.; Songsasen A. Synthesis of Cobalt Oxides Thin Films Fractal Structures by Laser Chemical Vapor Deposition, Sci. World J. 2014, 1-6

(15) Manteghi, F.; Kazemi, S. H.; Peyvandipour, M.; Asghari, A. Preparation and Application of Cobalt Oxide Nanostructures as Electrode Materials for Electrochemical Supercapacitors. RSC Adv. 2015, 5, 76458-76463.

(16) Wu, Z.; Zhu, Y.; Ji, X. NiCo2O4 based Materials for Electrochemical Supercapacitors. J. of Mater. Chem. A. 2014, 2, 14759–14772.

(17) Ling, T., Yan, D. Y., Jiao, Y., Wang, H., Zheng, Y., Zheng, X., ... & Qiao, S. Z. Engineering surface atomic structure of single-crystal cobalt (II) oxide nanorods for superior electrocatalysis. *Nature communications*, 2016, *7*, 12876.

(18) Huang, G.; Chen, T.; Wang, Z.; Chang, K.; Chen, W. Synthesis and Electrochemical
Performances of Cobalt Sulfides/Graphene Nanocomposite as Anode Material of Li-Ion
Battery, J. Power Sources, 2013, 235, 122-128.

(19) Wang, Y., Wu, J., Tang, Y., Lü, X., Yang, C., Qin, M., ... & Zhang, X. Phase-controlled synthesis of cobalt sulfides for lithium ion batteries. *ACS applied materials & interfaces*, 2012, *4*(8), 4246-4250.

(20) Chen, H.; Kung, C.; Tseng, C.; Wei, T.; Sakai, N.; Morita, S.; Ikegama, M.; Miyasaki, T.; Ho, K. Plastic Based Dye-Sensitized Solar Cells Using Co9S8 Acicular Nanotube Arrays as the Counter Electrode. J. Mater. Chem., A. 2013, 1, 13759-13768.

(21) Kristl, M., Dojer, B., Gyergyek, S., & Kristl, J. (2017). Synthesis of nickel and cobalt sulfide nanoparticles using a low cost sonochemical method. *Heliyon*, *3*(3), e00273.

(22) Yuan, X., Yin, J., Liu, Z., Wang, X., Dong, C., Dong, W., ... & Huang, F. Charge-Transfer-Promoted High Oxygen Evolution Activity of Co@ Co9S8 Core–Shell Nanochains. *ACS applied materials & interfaces*, 2018, 10(14), 11565-11571.

(23) You, B., Jiang, N., Sheng, M., & Sun, Y. Microwave vs. solvothermal synthesis of hollow cobalt sulfide nanoprisms for electrocatalytic hydrogen evolution and supercapacitors. *Chemical Communications*. 2015, 51(20), 4252-4255.

(24) Chen, Q., Li, H., Cai, C., Yang, S., Huang, K., Wei, X., & Zhong, J. In situ shape and phase transformation synthesis of Co 3 S 4 nanosheet arrays for high-performance electrochemical supercapacitors. *Rsc Advances*. 2013, 3(45), 22922-22926.

(25) Hu, Q. R.; Wang, S. L.; Zhang, Y.; Tang, W. H. Synthesis of Cobalt Sulfide Nanostructures by a Facile Solvothermal Growth Process. J. Alloys Compd. 2010, 491, 707–711.

(26) Ranaweera, C. K., Wang, Z., Alqurashi, E., Kahol, P. K., Dvornic, P. R., Gupta, B. K., ... & Gupta, R. K. Highly stable hollow bifunctional cobalt sulfides for flexible supercapacitors and hydrogen evolution. *Journal of Materials Chemistry A*. 2016, 4(23), 9014-9018.

(27) Feng, X., Jiao, Q., Liu, T., Li, Q., Yin, M., Zhao, Y., ... & Zhou, W. Facile Synthesis of Co9S8 Hollow Spheres as a High-Performance Electrocatalyst for the Oxygen Evolution Reaction. *ACS Sustainable Chemistry & Engineering*. 2017, 6(2), 1863-1871.

(28) Martin Chaplin. Electrolysis of Water. *water structure and scince.*2012.

(29) Su, D., Xie, X., Munroe, P., Dou, S., & Wang, G. Mesoporous hexagonal Co 3 O 4 for high performance lithium ion batteries. *Scientific reports*. 2014, 4, 6519.

(30) Meher, S. K., & Rao, G. R. Ultralayered Co3O4 for high-performance supercapacitor applications. *The Journal of Physical Chemistry C*. 2011, 115(31), 15646-15654.

(31) Pengfei, Y., Lili, S., Xiangyu, H., Chuanhui, X., Haiying, W., & Feng, W. Controlled Synthesis of Cobalt Sulfide Nanocrystalline by Ultrasonic Spray Pyrolysis Process. *Rare Metal Materials and Engineering*, 2016, 45(7), 1700-1704.

(32) Li, B., Hu, Y., Li, J., Liu, M., Kong, L., Hu, Y., & Kang, L. Mechanical alloying synthesis of Co9S8 particles as materials for supercapacitors. *Metals*. 2016, 6(6), 142.

(33) Pengfei, Y., Lili, S., Xiangyu, H., Chuanhui, X., Haiying, W., & Feng, W. Controlled Synthesis of Cobalt Sulfide Nanocrystalline by Ultrasonic Spray Pyrolysis Process. *Rare Metal Materials and Engineering*. 2016, *45*(7), 1700-1704.

(34) Xiong, D., Zhang, Q., Thalluri, S. M., Xu, J., Li, W., Fu, X., & Liu, L. One-Step Fabrication of Monolithic Electrodes Comprising Co9S8 Particles Supported on Cobalt Foam for Efficient and Durable Oxygen Evolution Reaction. *Chemistry–A*

European Journal. 2017,*23*(36), 8749-8755.

(35) Wang, Q., Jiao, L., Du, H., Si, Y., Wang, Y., & Yuan, H. Co 3 S 4 hollow nanospheres grown on graphene as advanced electrode materials for supercapacitors. *Journal of Materials Chemistry*. 2012,*22*(40), 21387-21391.

(36) Ranaweera, C. K., Zhang, C., Bhoyate, S., Kahol, P. K., Ghimire, M., Mishra, S. R., ... & Gupta, R. K. Flower-shaped cobalt oxide nano-structures as an efficient, flexible and stable electrocatalyst for the oxygen evolution reaction. *Materials Chemistry Frontiers*. 2017, 1(8), 1580-1584.

(37) J. Mujtaba, H. Sun, G. Huang, Y. Zhao, H. Arandiyan, G. Sun, S. Xu, J. Zhu, Co9S8
nanoparticles encapsulated in nitrogen-doped mesoporous carbon networks with improved lithium storage properties, RSC Adv. 6 (2016) 31775–31781.

(38) Gu, W., Hu, L., Hong, W., Jia, X., Li, J., & Wang, E. Noble-metal-free Co 3 S 4–S/G porous hybrids as an efficient electrocatalyst for oxygen reduction reaction. *Chemical Science*. 2016, *7*(7), 4167-4173.

(39) Hu, J., Qian, F., Song, G., Li, W., & Wang, L. Ultrafine MnO2 nanowire arrays grown on carbon fibers for high-performance supercapacitors. *Nanoscale research letters*. 2016, *11*(1), 469.

(40) Garg, N., Basu, M., & Ganguli, A. K. Nickel cobaltite nanostructures with enhanced supercapacitance activity. *The Journal of Physical Chemistry C*. 2014, *118*(31), 17332-17341.

(41) Ji, D. L., Li, J. H., Chen, L. M., Zhang, D., Liu, T., Zhang, N., ... & Liu, X. H. Needle-like CoO nanowires grown on carbon cloth for enhanced electrochemical properties in supercapacitors. *RSC Advances*. 2015, *5*(52), 41627-41630.

(42) Nagaraju, G., Ko, Y. H., & Yu, J. S. Self-assembled hierarchical β-cobalt hydroxide nanostructures on conductive textiles by one-step electrochemical deposition. *CrystEngComm*. 2014, 16(48), 11027-11034.

(43) Jiang, H., Yang, L., Li, C., Yan, C., Lee, P. S., & Ma, J. High–rate electrochemical capacitors from highly graphitic carbon–tipped manganese oxide/mesoporous carbon/manganese oxide hybrid nanowires. *Energy & Environmental Science*. 2011, 4(5), 1813-1819.

(44) Masikhwa, T. M., Madito, M. J., Bello, A., Lekitima, J., & Manyala, N. Microwave-assisted synthesis of cobalt sulphide nanoparticle clusters on activated graphene foam for electrochemical supercapacitors. *RSC Advances*. 2017, 7(33), 20231-20240.

(45) Jin, M., Lu, S. Y., Ma, L., Gan, M. Y., Lei, Y., Zhang, X. L., ... & Yan, M. F. Different distribution of in-situ thin carbon layer in hollow cobalt sulfide nanocages and their application for supercapacitors. *Journal of Power Sources*. 2017, 341, 294-301.

(46) Moosavifard, S. E., Kaverlavani, S. K., Shamsi, J., & Bakouei, A. Hierarchical multi-shelled nanoporous mixed copper cobalt phosphide hollow microspheres as a novel advanced electrode for high-performance asymmetric supercapacitors. *Journal of Materials Chemistry A*. 2017, 5(35), 18429-18433.

(47) Hu, J ; Qian, F; Song, G ;Li, W;Wang, L .Ultrafine MnO2Nanowire Arrays Grown
on Carbon Fibers for High-Performance Supercapacitors. Nanoscale Research Letters,
2016, 1-6.

(48) Gervas, C., Khan, M. D., Zhang, C., Zhao, C., Gupta, R. K., Carleschi, E., ... & Revaprasadu, N. Effect of cationic disorder on the energy generation and energy storage applications of Ni x Co 3− x S 4 thiospinel. *RSC Advances*. 2018, 8(42), 24049-24058.

(49) Chauhan, M., Reddy, K. P., Gopinath, C. S., & Deka, S. Copper Cobalt Sulfide Nanosheets Realizing a Promising Electrocatalytic Oxygen Evolution Reaction. *ACS Catalysis*. 2017, *7*(9), 5871-5879.

(50) Yang, Z., Zhang, J. Y., Liu, Z., Li, Z., Lv, L., Ao, X., ... & Wang, C. "Cuju"-Structured Iron Diselenide-Derived Oxide: A Highly Efficient Electrocatalyst for Water Oxidation. *ACS applied materials & interfaces*. 2017, 9(46), 40351-40359.

(51) Wu, L., Zhang, K., Wang, T., Xu, X., Zhao, Y., Sun, Y., ... & Du, Y. Cobalt Sulfide Nanotubes (Co9S8) Decorated with Amorphous MoS x as Highly Efficient Hydrogen Evolution Electrocatalyst. *ACS Applied Nano Materials*. 2018, *1*(3), 1083-1093.

(52) Zhang, C.; Wang, Z.; Bhoyate, S.; Morey, T.; Neria, B.; Vasiraju, V.; Gupta, G.; Palchoudhury, S.; Kahol, P.; Mishra, S.; et al. MoS2 Decorated Carbon Nanofibers as
Efficient and Durable Electrocatalyst for Hydrogen Evolution Reaction. C 2017, 3, 33.

(53) Hui, L., Xue, Y., Jia, D., Zuo, Z., Li, Y., Liu, H., ... & Li, Y. Controlled Synthesis of a Three-Segment Heterostructure for High-Performance Overall Water Splitting. *ACS applied materials & interfaces*. 2018, 10(2), 1771-1780.

(54) Zhang, G., Feng, Y. S., Lu, W. T., He, D., Wang, C. Y., Li, Y. K., ... & Cao, F. F.

(2018). Enhanced Catalysis of Electrochemical Overall Water Splitting in Alkaline Media by Fe Doping in Ni3S2 Nanosheet Arrays. *ACS Catalysis*. 2018, 8(6), 5431-5441.

(55) Deng, T., Zhang, W., Arcelus, O., Kim, J. G., Carrasco, J., Yoo, S. J., ... & Cui, X. Atomic-level energy storage mechanism of cobalt hydroxide electrode for pseudocapacitors. *Nature communications*.2017, *8*, 15194. For CoOH equasion.

(56) Patil, S. J., Kim, J. H., & Lee, D. W. Graphene-nanosheet wrapped cobalt sulphide as a binder free hybrid electrode for asymmetric solid-state supercapacitor. *Journal of Power Sources*, 2017. *342*, 652-665.

(57) Alqurashi, E. Facile Synthesis and Electrochemical Analysis of Cobalt Sulfide Nanostructures for Supercapacitor Applications, 2015.

(58) Alqahtani, D. Effect of Metal Ion Substitution on Electrochemical Properties of Cobalt Oxide for Energy Applications, 2017.